**Article:**
Chai, Y., Gao, N., Wang, M. et al. (2020) H2 production from co-pyrolysis/gasification of waste plastics and biomass under novel catalyst Ni-CaO-C. Chemical Engineering Journal, 382. 122947. ISSN: 1385-8947

https://doi.org/10.1016/j.cej.2019.122947

# $H_2$ Production from Co-pyrolysis/gasification of Waste Plastics and Biomass under Novel Catalyst Ni-CaO-C

Yue Chai[a], Ningbo Gao[b,*], Meihong Wang[a,*], Chunfei Wu[c]

*a. Department of Chemical and Biological Engineering, The University of Sheffield, Mappin Street, Sheffield, S1 3JD, UK.*

*b. School of Energy and Power Engineering, Xi'an Jiaotong University, 28 Xianning West Road, Xi'an, China.*

*c. School of Chemistry and Chemical Engineering, Queen's University Belfast, University Road, Belfast, BT7 1NN, UK.*

**Abstract**

Energy security and environmental pollution have been important topics over the world. With depletion of traditional fossil fuels, it is necessary to find new kinds of substitute energies that are green and renewable. Co-pyrolysis/gasification of mixture of waste (i.e. plastics) and biomass is a potential solution and $H_2$ is an ideal energy carrier with wide range of use. This paper aims to develop a new catalyst Ni-CaO-C and to examine its performance under optimal operating conditions of pyrolysis/gasification of plastics and biomass for $H_2$ production. Experimental studies adjusting Ni loads and support ratios of catalyst were performed to explore the catalytic activity and $CO_2$ adsorption capability of the new catalyst. Operating conditions such as feedstock ratio, pyrolysis temperature, reforming temperature and water injection flowrate were also examined experimentally to find optimal operating conditions. Consequently, experiment results indicated that high $H_2$ production (86.74 mol% and 115.33 mmol/g) and low $CO_2$ concentration (7.31 mol%) in the gaseous products can be achieved with new catalyst Ni-CaO-C under the optimal operating conditions. Therefore, this study points to effective new approaches to increase $H_2$ production from the pyrolysis/gasification of waste plastics and biomass.

Keywords: Pyrolysis and Gasification; Biomass; Plastics; Catalyst; $H_2$ Production

## 1.Introduction

### 1.1 Background

Energy security and environmental pollution have been important topics all over the world (Jacobson, 2008). For energy security, with depletion of fossil fuels, excessive dependence on this traditional energy raises serious problems in energy supply. For environmental pollution, consumption of fossil fuels releases greenhouses gases (GHG) (especially for $CO_2$) into atmosphere, resulting in climate change and global warming (Déparrois et al., 2019). In addition to gaseous emissions, significant amount of solid wastes such as waste plastics is also discarded every year. To solve these two problems, pyrolysis/gasification of plastics and biomass for $H_2$ production is ideal to provide energy sustainably at low environment cost.

Plastics is one typical solid waste with considerable discarded annually over the wold. Normally, plastics is a complicated polymer material with high molecular weight, which is difficult to be naturally decomposed (Verma et al., 2016). Hence new technologies to treat waste plastics effectively keep attracting interest of researchers worldwide. During pyrolysis/gasification process, plastics can be decomposed for $H_2$ production within minutes at high efficiency. However, plastics is easily melted and stuck on the surface of reactor tube to restrict continuous feed of fresh plastics (Block et al.,2018).

Biomass is a renewable energy source, which could realise a carbon neutral process when being used for energy supply (Yao et al., 2018). It is reported that bioenergy accounted for two-thirds of primary renewable energy production in 2014 in Europe, and it will continue remaining a key energy source beyond 2030 (IRENA, 2018). Biomass is one of the mostly used feedstock for pyrolysis/gasification. In previous studies, when only biomass was used for pyrolysis/gasification, low $H_2$ production and high char yield were observed due to the high oxygen content of biomass (Alvarez et.al., 2014). Pyrolysis/gasification of mixture of plastics and biomass for $H_2$ production is an ideal solution to solve problems of energy security and environmental pollution at the same time. The advantages of this technology can be summarised from two aspects.

From feedstock aspect, biomass is renewable resource without worry of depletion (Basu, 2013). Waste plastics is decomposed thoroughly with high efficiency. Co-pyrolysis/gasification of plastics and biomass makes it possible for continuous feed, and char derived from biomass could promote decomposition of plastics furthermore (Zhang et al., 2016). From the product aspect, $H_2$ is obtained for energy use, and less emission is released, alleviating the burden on environment. In addition, compared to pyrolysis/gasification of only plastics or biomass, higher $H_2$ production and lower tar/char yields are realised because the high H/C of plastics can compensate the high oxygen composition of biomass (Block et al.,2018).

In order to make the most use of synergic effects of plastics and biomass, catalyst is introduced to promote products distribution and yields (especially for $H_2$) significantly. Nowadays, the research focus in pyrolysis/gasification of waste plastics and biomass is to develop new catalyst with high performance.

### 1.2 Motivations for this study

$H_2$ is one of the main gas products from pyrolysis/gasification of plastics and biomass with various advantages. Firstly, $H_2$ is an ideal energy carrier, whose lower heating value could reach 12.7 $MJ/m^3$. Secondly, $H_2$ is a clean and renewable energy. Combustion of $H_2$ only produces water without GHG emissions. Thirdly, $H_2$ has a wide range of uses and high economic value (Kumar et al., 2009). For example, $H_2$ could be directly combusted or be used in fuel cell for energy supply. It can also be used for Fisher-Tropsch synthesis to generate liquid fuels (Al-Rahbi and Williams, 2017). Utilisation of $H_2$ for energy has a bright future. To evaluate the $H_2$ production, both $H_2$ yield and $H_2$ composition in gas products are important indexes. Improving the $H_2$ production with high $H_2$ yield and composition from pyrolysis/gasification process is the main driver for this study.

Catalyst plays a key role in the pyrolysis/gasification process (Kwon et al., 2018). Nickel is normally used as active core to increase the reaction rate and extent thus higher gas yields, and it can be attached on various supports such as $Al_2O_3$, Co, foam ceramic and so on (Sikatwar et al., 2017). Due to the specific chemical or physical

characteristics of different supports, the catalyst could be modified to have different properties. Finding a new catalyst resulting in better $H_2$ production with high $H_2$ yield and composition from pyrolysis/gasification of mixture of plastic and biomass is the first motivation of this study.

Operating conditions are important to influence the product yields of pyrolysis/gasification process (Block et al.,2018). Inappropriate operating conditions could restrict activity of catalyst and reaction extent of reactions, thus decreasing the product yields. A comprehensive analysis is necessary to find optimal operating conditions to achieve better product yields, which is the second motivation of this study.

### 1.3 Aim of this study

This study aims to develop a new catalyst Ni-CaO-C, and to evaluate its catalytic activity and $CO_2$ adsorption capability for pyrolysis and gasification of plastics and biomass. Furthermore, optimal operating conditions (i.e. feedstock ratio, pyrolysis temperature, reforming temperature and water injection flowrate) under the new Ni-CaO-C catalyst are also investigated.

### 1.4 Novel contribution of this study

The novelties of this study include:

(a) In previous studies, only CaO or activated carbon was used as catalyst or catalyst support to load Ni (in Table 1). In this study, a new dual-support catalyst Ni-CaO-C (combining CaO and activated carbon to support Ni as active core) was synthesised for pyrolysis/gasification of mixture of plastics and biomass.

From Table 1, all these previous studies are for $H_2$ production. CaO has desired ability to absorb $CO_2$, which helps to increase the $H_2$ composition effectively. However, CaO is quite weak to promote gas yields. Activated carbon is active to participate in most reactions in the reforming stage and it also has perfect pore structure and nice reduction effects for active core Ni. These characteristics could promote gas yield (including $H_2$ yield) effectively, but the $H_2$ composition becomes low correspondingly due to high yields of other gas products (e.g. $CO_2$). So far, there is no study combining CaO and activated carbon as catalyst support together. In this study, a new dual-support

116 catalyst Ni-CaO-C (combining CaO and activated carbon to support Ni as active core)
117 was synthesised for pyrolysis/gasification of mixture of plastics and biomass. The
118 synergic effects between Ni, CaO and activated carbon will be investigated to see
119 whether the $H_2$ production can be improved (with both high $H_2$ yield and composition).
120 This is the main novelty of this study.

121 **Table 1 Previous studies on different catalysts used in gasification**

| Publications | Catalyst | Feedstock(s) | Agent | Equipment | Application |
|---|---|---|---|---|---|
| Hu and Huang (2009) | CaO | Wet biomass (Pine sawdust) | Steam | One-stage fixed bed reactor | Hydrogen production |
| Acharya et al. (2010) | CaO | Biomass (Pine sawdust) | Steam | One-stage fixed bed reactor (Stainless steel cylinder tube) | Hydrogen production |
| Wu and Williams (2010a) | Ni-Mg-Al-CaO | Plastic (polypropylene) | Steam | Two-stage fixed bed reactor | Hydrogen production |
| Kumagai et al. (2015) | Ni-Mg-Al-Ca | Biomass and plastic (Wood sawdust and polypropylene) | Steam | Two-stage fixed bed reactor | Hydrogen production |
| Liu et al. (2018) | $Fe_2O_3$, CaO | Microalgae | Air | One-stage fixed bed reactor | Hydrogen production |
| Cho et al. (2015) | Ni-C, $Fe_2O_3$, MgO, $Al_2O_3$ | Plastic (PVC) | Air | One-stage fluidised bed reactor | Hydrogen production |
| Ren et al. (2017) | Ni-C | Biomass volatiles (from corn hub pyrolysis ) | Steam | Two-stage fixed bed reactor | Hydrogen production |

122 (b) Optimal operating conditions under the new Ni-CaO-C catalyst were also
123 investigated, which tests the practical performance of new catalyst. A better $H_2$
124 production was realised eventually. This may inspire further studies by other
125 researchers in the same field.

126 **2. Materials and methods**

127 **2.1 Materials**

128 Pure low density polyethylene (LDPE) particulates with size smaller than 5 mm were
129 selected as plastic feedstock (provided by Shenhua Chemical Industry, China). The
130 biomass used in this study for pyrolysis/gasification is pine sawdust, which was
131 processed with a filter of 60 mesh. The results of proximate and ultimate analysis of
132 biomass are shown in Table 2. The ultimate analysis of plastics is shown in Table 3.
133 Due to pure LDPE used, it is not necessary to perform proximate analysis for the plastic

feedstock since most components of pure LDPE are volatiles, reaching nearly 99 wt% (Zhou et al., 2014).

Pure plastics is used in this study because real plastic wastes are complicated in compositions of different types of plastics. At present, the main task is to examine the performance of new catalyst, using waste plastics could disturb analysing the properties of new catalyst. In future, the results of using pure plastics for co-pyrolysis/gasification could be standard to instruct practical application when treating real plastic waste. LDPE is one of the most widely used plastics with good representativeness (Czajczyńska et al., 2017). Pine sawdust is also one of the most widely used biomass for pyrolysis/gasification in previous studies (Alvarez et al., 2014).

**Table 2 Results of proximate and ultimate analysis of biomass (Pine sawdust)**

| Proximate analysis | | Ultimate analysis | |
|---|---|---|---|
| Moisture | 2.77 wt% | C | 49.17 wt% |
| Fixed carbon | 13.91 wt% | H | 6.36 wt% |
| Volatile matter | 82.03 wt% | O | 44.12 wt% |
| Ash | 1.29 wt% | N | 0.36 wt% |

**Table 3 Results of ultimate analysis of plastics (LDPE)**

| Ultimate analysis | |
|---|---|
| C | 85.38 wt% |
| H | 14.62 wt% |
| O | 0 wt% |
| N | 0 wt% |

The other chemicals used in the experiments are shown below:

$Ni(NO_3)_2.6H_2O$ (provided by Tianjin Yongshen Fine Chemical Ltd., China) is used to provide nickel content for Ni-CaO-C catalyst. CaO was obtained by calcining calcium acetate (Provided by Chengdu Kelong Chemical Ltd., China) in muffle furnace under 850 ºC for 2 hours. Activated carbon was obtained from potassium hydroxide and petroleum coke using activation method. Ammonia solution (25 wt%) is provided by Tianjin Tianli Chemical Ltd., China.

## 2.2 Catalyst preparation

Appropriate catalyst preparation methods were selected. The performance when using three different methods (i.e. impregnation method (Yang et.al., 2018), rising pH method and sol-gel method (Liu and Au, 2002; Zhang et.al., 2007)) was compared, rising pH method was eventually selected as the catalyst preparation method. Details

about rising pH method were introduced in Kumagai et al. (2015). The specific amount (i.e. based on different Ni load) of $Ni(NO_3)_2.6H_2O$ was dissolved in deionized $H_2O$. $NH_3.H_2O$ with concentration 1 mol/L was added into the solution for precipitation drop by drop under 40 ºC and moderate stirring. In the end, pH of the solution should reach 8.3. The transparent solution became turbid after precipitation. After static settlement, the solution was separated into two layers. The top transparent liquid was removed and deionized water was added until the total solution was 200 mL. Specific amount of CaO and activated carbon was added into the solution under moderate stirring. Stirring was maintained for 12 h for uniform mixture of components. Then the solution was dried at 105 ºC overnight (nearly 10 h) and the precursor was calcined under $N_2$ atmosphere at 750 ºC for 3 h.

### 2.3 Experimental System

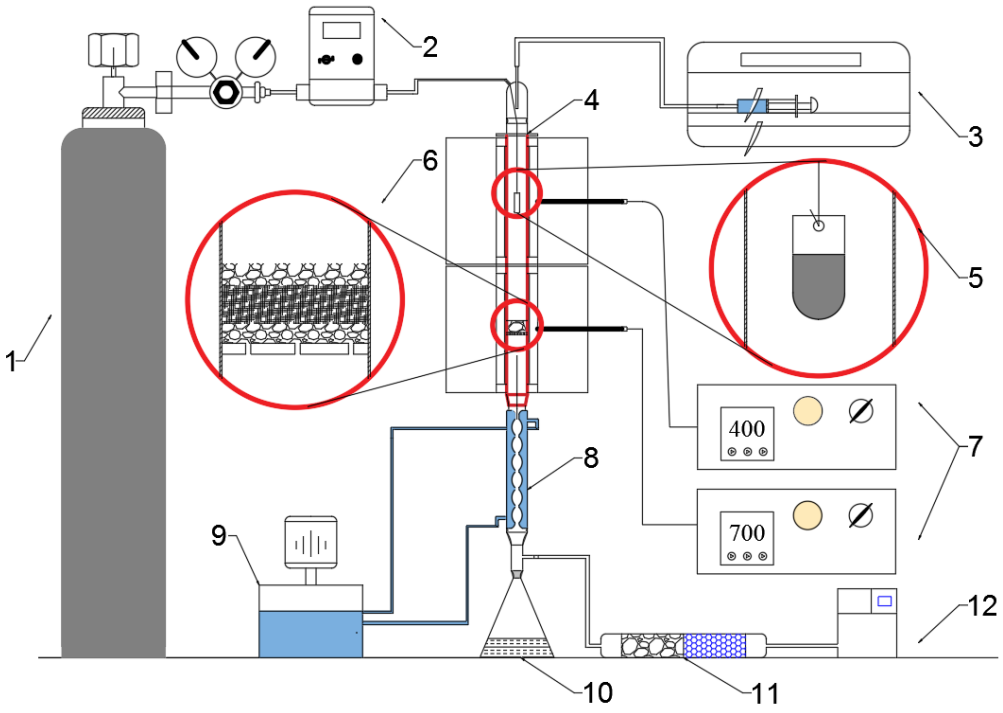


**Figure 1 Two-stage fixed bed pyrolysis/gasification system (Gao et al., 2018)**

(1. Nitrogen cylinder, 2. Mass flowmeter, 3. Microinjection pump, 4. Quartz reaction tube and heating furnaces (***Top: pyrolysis stage; Bottom: reforming stage***), 5. Quartz crucible, 6. Catalytic layer: quartz wool + catalyst, 7. Temperature controllers, 8. Condenser pipe, 9. Cooling water and water pump, 10. Conical flask, 11. Dryer, 12. Gas chromatography (GC) or on-line GC)

176 The equipment used for pyrolysis/gasification is a two-stage fixed bed reactor, which
177 was designed and commissioned at Xi'an Jiaotong University. The central diameter of
178 each stage of rector is 30 mm, and the height of each stage is 150 mm. From Figure 1,
179 the feedstock is placed in the upper stage inside a quartz crucible where pyrolysis starts.
180 The catalyst is fixed in the bottom stage, and reforming reactions as well as cracking
181 reactions take place when volatiles go through the catalyst layer. Both stages have their
182 own temperature controllers, which allow separately heating. Water is injected from the
183 top of the reactor to serve as gasification agent.
184 The experiment procedures are described as following:
185 (a) 1.0 g of catalyst was put on top of the quartz wool in the bottom stage (i.e. *symbol*
186 *6* in Figure 1). 0.5 g mixture of LDPE and pine sawdust were well mixed and put in the
187 quartz crucible (i.e. *symbol 5*).
188 (b) $N_2$ was firstly injected into the system at the flow rate of 60 mL/min for 15 ~ 20
189 min to ensure a no-oxygen environment (i.e. *symbol 2*). Then the bottom stage was pre-
190 heated to the specific required temperature with constant heating rate (30 ºC/min) (i.e.
191 *symbol 7 bottom temperature controller*).
192 (c) After the temperature of bottom stage was kept stable, the upper stage started to
193 be heated (30 ºC/min) (i.e. *symbol 7 upper temperature controller*). When the upper
194 stage temperature reached 100 ºC, the water started to be injected to the system with
195 specific injection flowrate by switching on the water pump (i.e. *symbol 3*).
196 (d) The ice water-cooling system began to work (i.e. *symbol 9*), while the product
197 gases went through drying system (i.e. *symbol 11*) and started to be collected at the
198 same time. The whole pyrolysis/gasification experiment could last for 1 hour.
199 (e) Depending on the analytical instrument to use, different gases collection methods
200 were utilised. When a gas chromatography (GC) would be used. Gas collection bag was
201 connected after the dryer (i.e. *symbol 11*). After one-hour reaction, the gas collection
202 stopped and the product gases in gas collection bag were examined by the GC (GC7900,
203 Tianmei Ltd., China). Alternatively, an on-line gas chromatography (ETG Ltd., Italy)
204 is sometimes used to measure the dynamic state of outlet gas compositions. The gas

outlet after dryer (i.e. *symbol 11*) was directly connected with online analyser and no gas collection bag was used. Only limited number of catalysts were chosen to investigate the real-time gas yields situations using on-line gas chromatography.

### 2.4 Characterisation of catalysts

Thermogravimetric analysis (TGA) was carried out by a thermogravimetric analyser (SHIMADZU, Japan) to analyse the coke formation of used catalyst. Nearly 10 mg of samples was heated at 10 ºC/min under the air atmosphere from room temperature to 800 ºC, and the temperature was kept stable at 800 ºC for 10 mins before decreasing. X-ray diffraction (XRD) was performed using a Bruker D8 ADVANCE (Bruker Ltd., Shaanxi, China) to detect the existing chemicals on the fresh and used catalysts. The change range of 2 theta angle is from 20° to 90°. Scanning electron microscope (SEM) was used to detect the microstructure of the used catalyst, and energy dispersive X-ray (EDX) was used to measure the element distribution on used catalyst. The SEM and EDX analysis were all performed on GeminiSEM 500 (Carl Zeiss Ltd., Shanghai, China). Brunauer Emmett Teller (BET) analysis was carried to detect the specific surface area of fresh catalysts using JW-BK200 (JINGWEIGAOBO Ltd., Beijing, China). Temperature programme reduction (TPR) was performed using a DAS-7000 (Huasi Ltd., Hunan, China) under 3 mol% $H_2$ flow to detect the reducibility of catalyst.

## 3. Experimental studies of catalyst effectiveness

In this section, the catalytic activity for $H_2$ production and $CO_2$ absorption capability of the Ni-CaO-C catalyst are investigated by changing the Ni load and support ratios. The specific experimental plan is listed in Table 4. It should be noted that the main objective of this study is to improve $H_2$ production. Thus only results of gas yields and compositions are provided and the results of other products including tar and char are ignored.

**Table 4 List of experimental studies for catalyst effectiveness**

| Exp. Number | (1) | (2) | (3) | (4) | (5) | (6) | (7) | (8) | (9) |
|---|---|---|---|---|---|---|---|---|---|
| Ni load (wt%) | 0 | 10% | 10% | 5% | 10% | 15% | 20% | 10% | 10% |
| CaO : C (weight ratio) | 0 | 10:0 | 0:10 | 5:5 | 5:5 | 5:5 | 5:5 | 3:7 | 7:3 |

*** In Exp. (10), Ni-$Al_2O_3$ catalyst was used. Ni load is still 10 wt%, and $Al_2O_3$ is used as support, which is prepared using wet impregnation method.**

****For Exp. (1) ~ (10), operating conditions are listed here: feedstock ratio (Biomass:Plastic) 5:5; T of pyrolysis stage 700 ºC; T of reforming stage 600 ºC; water injection flowrate 5 mL/h.**

### 3.1 Influence of Ni load on catalytic activity

In gasification, *Reactions 1 - 5* take place (Higman and Burgt, 2008). As the active core, Ni content (Ni/NiO) serves to improve the reaction rates of cracking condensable volatiles (tar), reforming reactions (*Reactions 4 and 5*) and other reactions (*Reactions 1 – 3*). Different loads of Ni in catalyst influence the gas yields. Five different Ni loads ranging from 0 wt% to 20 wt% were tested to investigate the influence of Ni load on catalytic activity.

**Water – Gas Reaction :** $C + H_2O \leftrightarrow CO + H_2$ **+131 MJ/kmol Reaction 1**

**Boudouard Reaction :** $C + CO_2 \leftrightarrow 2CO$ **+172 MJ/kmol Reaction 2**

**Methanation Reaction :** $C + 2H_2 \leftrightarrow CH_4$ **-75 MJ/kmol Reaction 3**

**Water-Gas-Shift Reaction:** $CO + H_2O \leftrightarrow CO_2 + H_2$ **-41 MJ/kmol Reaction 4**

**Steam-Methane-Reforming Reaction:** $CH_4 + H_2O \leftrightarrow CO + 3H_2$ **+206 MJ/kmol Reaction 5**

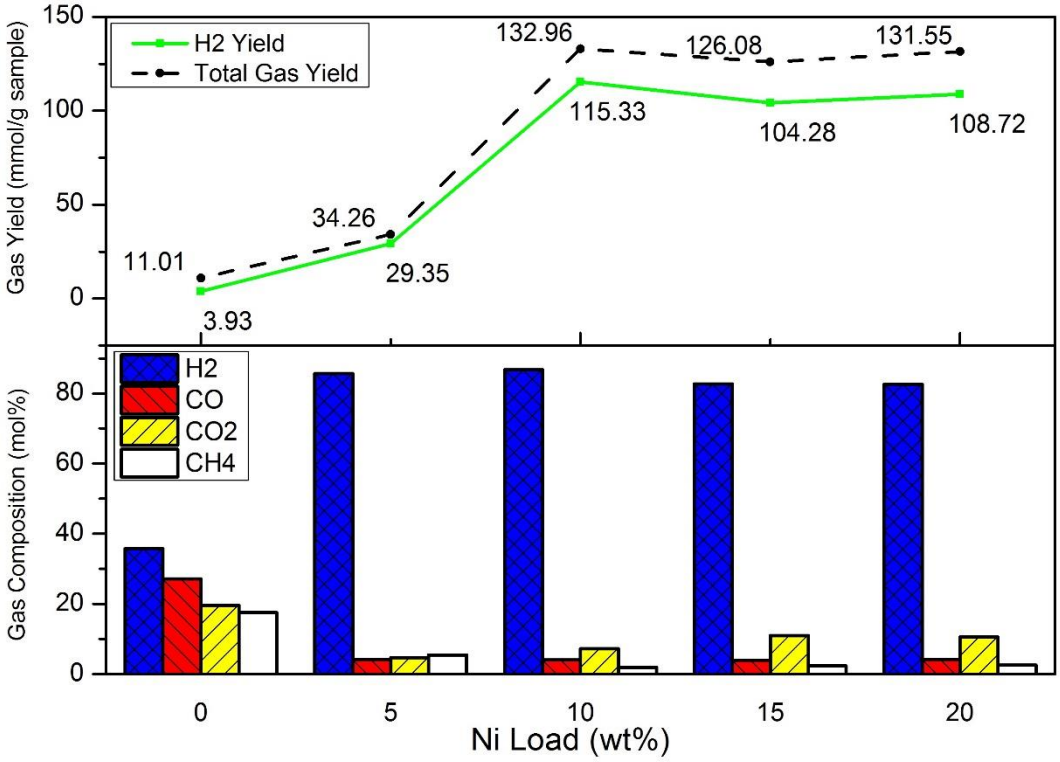


**Figure 2 Gas compositions and yields when changing Ni load from 0 wt% to 20 wt% (When Ni load from 5 to 20 wt%: with all CaO:C = 5:5, Biomass:Plastic=5:5, Pyrolysis T: 700 ºC,**

**Reforming T: 600 ºC, Water: 5 mL/h)**

***Total gas yield is the sum of $H_2$, $CO_2$, CO and $CH_4$ production. The *total gas yield* in this article all refer to this definition.**

In Figure 2, no catalyst is used in Exp. (1) (i.e. 0 wt% Ni load). Under this condition, $H_2$ composition and yield in gas mixture are only at 35.73 mol% and 3.93 mmol/g respectively. With introduction of 5 wt% Ni catalyst, $H_2$ composition reaches 85.68 mol%, but the $H_2$ yield is still relatively low at 29.35 mmol/g. The peak of both $H_2$ composition and yield are all achieved at 10 wt% Ni load at about 86.74 mol% and 115.33 mmol/g. Continuous increase of Ni load fails to promote the $H_2$ composition and yield furthermore.

The catalytic activity of Ni-CaO-C is demonstrated when comparing results with catalysts (i.e. Exp. (4) ~ (7)) and without catalysts (i.e. Exp. (1)). It is vital to validate that Ni-CaO-C catalyst indeed possesses ability to improve gas yields. Increasing trends of $H_2$ composition and yield could be observed when Ni load increases from 0 wt% to 10 wt%. When 5 wt% Ni catalyst is introduced, a limited promotion is realised. The probable reason is that 5 wt% Ni cannot reach the lowest active core content requirement for complete reactions. Insufficient Ni hinders the reaction extent of relevant reactions, and less $H_2$ is produced due to lower catalytic activity of catalyst. On the contrary, excessive Ni load also brings about negative influences. 15 wt% and 20 wt% Ni loads have worse performances compared to 10 wt%. A probable explanation might be that excessive Ni could result in metal agglomeration of active core with larger particle size and the integrated dispersion degree of Ni also decreases (Zhao et al., 2015). Consequently, the activity of catalyst could be restricted.

### 3.2 Influence of CaO:C ratio and support type on catalytic activity and $CO_2$ absorption capability

In order to investigate the catalytic activity and $CO_2$ absorption capability of new Ni-CaO-C catalyst, experiments with different CaO:C ratios as well as using $Al_2O_3$ as support were performed (i.e. Exp (2), (3), (5), (8), (9) and (10) in Table 4). The $H_2$ compositions and $H_2$ yields were measured as shown in Figure 3.

When only CaO was used as catalyst support along with 10 wt% Ni load in Exp. (2) (i.e. CaO:C=10:0). At this condition, $H_2$ composition is 88.89 mol% and $CO_2$

composition is 2.87 mol%. The total gas yield is at about 37.35 mmol/g with $H_2$ yield 33.20 mmol/g. It could be concluded that introduction of CaO as catalyst support has good performance to influence the gas compositions due to its $CO_2$ adsorption capability. *Reaction 6* indicates $CO_2$ adsorption process of CaO during pyrolysis/gasification process.

$$\mathbf{CaO + CO_2 \rightarrow CaCO_3} \qquad \textit{Reaction 6}$$

The generated $CO_2$ is adsorbed by CaO and $CO_2$ composition is alleviated directly, which elevates compositions of other gases straightforward. Furthermore, reduced $CO_2$ concentration is advantageous to move reaction equilibrium of water-gas-shift (WGS) reaction (*Reaction 4*) towards generating more $CO_2$ and $H_2$. With newly generated $CO_2$ being adsorbed by CaO continuously, the composition of $H_2$ can be further increased.

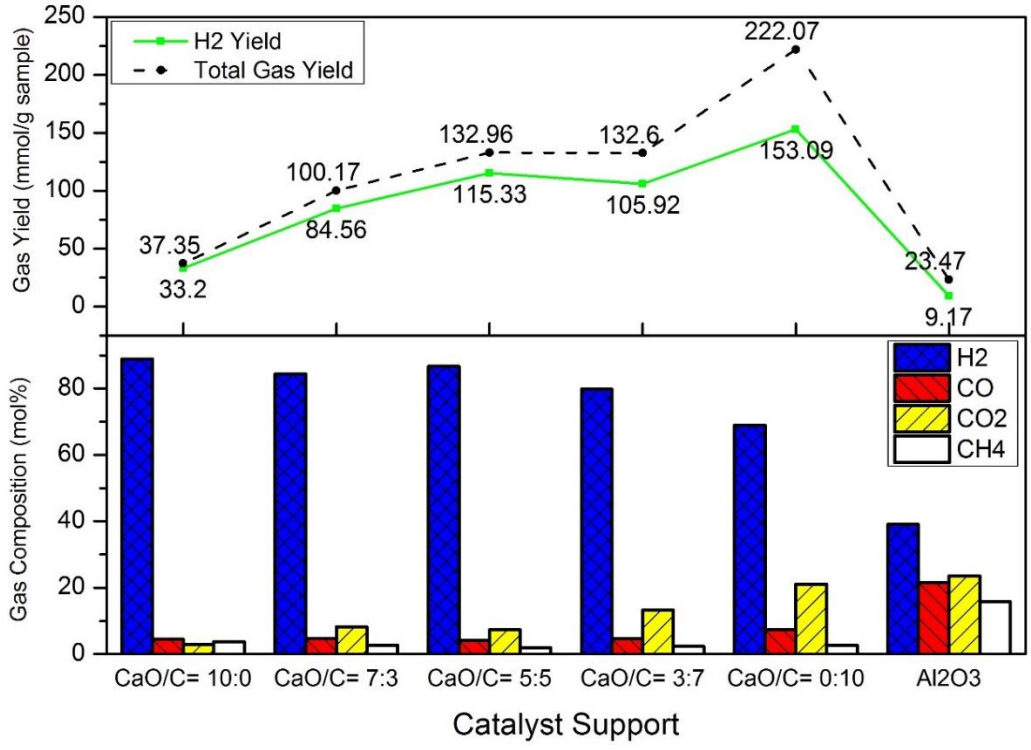


**Figure 3 Gas compositions and yields when changing CaO:C ratios and support type (For all cases Ni load: 10 wt%, Biomass:Plastic=5:5, Pyrolysis T: 700 ºC, Reforming T: 600 ºC, Water: 5 mL/h)**

When only activated carbon was used as catalyst support in Exp. (3) (i.e. CaO:C=0:10), the $H_2$ composition is 68.94 mol% and the total gas yield is 222.06 mmol/g with $H_2$ yield 153.09 mmol/g. The $H_2$ yield using activated carbon is nearly 5 times of that only using CaO. Activated carbon is active in reforming stage. It could be

observed that activated carbon directly takes part in series of reactions (*Reaction 1 - 3*). Water-Gas (WG) reaction (*Reaction 1*) helps to generate more CO and $H_2$, increasing $H_2$ yield directly. Boudouard reaction (*Reaction 2*) and methanation reaction (*Reaction 3*) improve the yields of CO and $CH_4$, which are reactants of WGS reaction and steam-methane-reforming (SMR) reaction. Increasing reactants concentration results in more product gases including $CO_2$ and $H_2$ due to movement of reaction equilibrium. The participation of activated carbon in reactions leads to enhancement of $H_2$ yield. In addition, the internal structure of activated carbon is another key factor influencing the gas yields. Activated carbon is an ideal catalyst support with abundant pore structure, providing sufficient specific surface area to load active core Ni and large inner space for catalytic reactions. Reactions including cracking of heavier molecules and reforming reactions are promoted effectively.

Considering characteristics of CaO and activated carbon, it is a good idea to use mixture of CaO and activated carbon as catalyst support. Under the same Ni load (i.e. 10 wt%), three different ratios of CaO:C including 7:3, 5:5 and 3:7 (Exp. (9), (5) and (8)) were investigated. In Figure 3, the $H_2$ compositions for different CaO:C ratios 7:3, 5:5 and 3:7 are 84.41 mol%, 86.74 mol% and 79.88 mol%. The $H_2$ yields are 84.56 mmol/g, 115.33 mmol/g and 105.92 mmol/g respectively. Relatively high $H_2$ composition and yield are observed due to synergistic effect of two supports and active core. The specific mechanism of synergic effects will be discussed in *section 3.3*.

As one of the most commonly used catalysts for pyrolysis/gasification, Ni-$Al_2O_3$ is selected for comparison. In Exp. (10), Ni-$Al_2O_3$ was used as catalyst with 10 wt% Ni load and $Al_2O_3$ support. The $H_2$ composition and $H_2$ yield are 39.09 mol% and 9.17 mmol/g. In another study using catalyst Ni-$Al_2O_3$ for co-pyrolysis/gasification of plastics (PP) and biomass (pine sawdust) (Alvarez et al., 2014), the highest $H_2$ composition and yield are at 52.10 mol% and 27.27 mmol/g when the reforming temperature is 800 ºC. Compared to the results using dual-support catalyst Ni-CaO-C, both $H_2$ composition and yield of Ni-$Al_2O_3$ in this study and in the study of Alvarez et al. (2014) are much lower. The advantages of new Ni-CaO-C catalyst are very obvious.

### 3.3 Mechanism of synergic effects of Ni-CaO-C catalyst

To summarise the specific function of different components in the catalyst Ni-CaO-C. Figure 4 is used to describe the synergetic effects of Ni-CaO-C on improving $H_2$ composition and yield. When volatiles from pyrolysis stage enter reforming stage, Ni/NiO (as the active core) serves to accelerate the reaction rates of different reactions by reducing activation energy, the total gas yields are promoted. At the same time, two supports also function to change the gas products distribution and yields according to their own properties. On one hand, activated carbon increases the total gas yield (including $H_2$ and $CO_2$ yields) due to its active participation in reactions in reforming stage and better pore structure. On the other hand, CaO is good at improving $H_2$ composition effectively. Generated $CO_2$ (under functions of Ni/NiO and activated carbon) is adsorbed when contacting with CaO, resulting in an increasing $H_2$ composition directly and promotion of WGS reaction (i.e. more $H_2$ generated). In addition, all the reactions occurring in reforming stage influence each other. The product for one reaction could be the reactant for another reaction and a dynamic equilibrium could be achieved with an overall trend to obtain a higher $H_2$ production. In summary, all the factors above work together to promote the $H_2$ composition and yield, demonstrating the catalytic activity and $CO_2$ adsorption capability of the dual–support catalyst Ni-CaO-C.

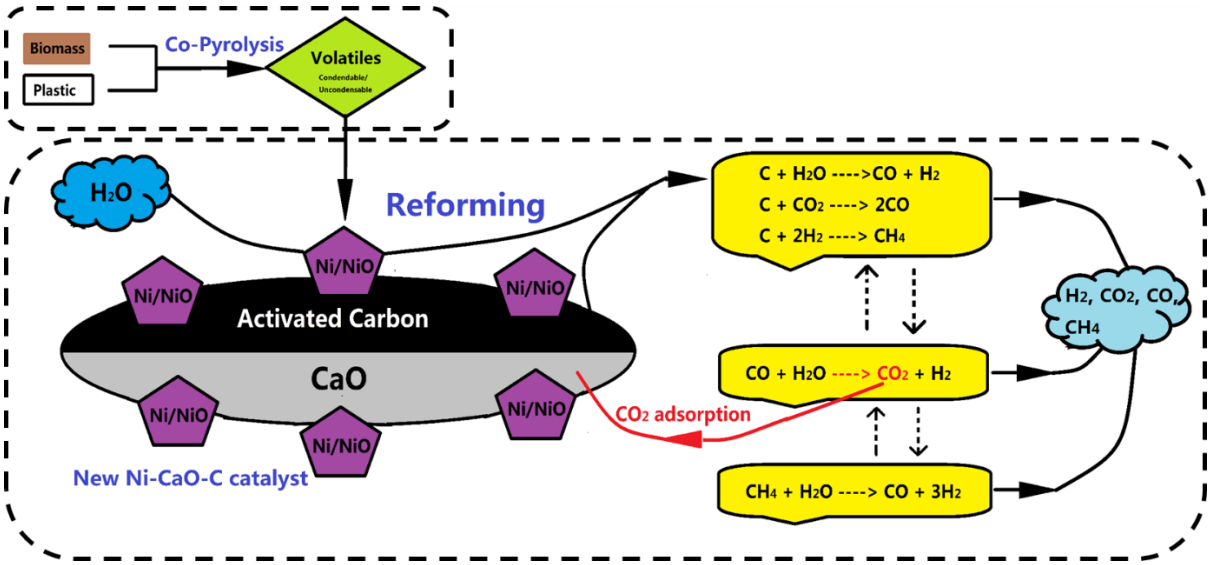


**Figure 4 Mechanism of Ni-CaO-C during pyrolysis/gasification of plastic and biomass (adapt from Kumagai et al., 2015)**

### 3.4 Real time experimental tests with on-line GC analysis

Three different catalysts including Ni-CaO, Ni-C and Ni-CaO-C (CaO:C=5:5) were selected (i.e. Exp. (2), Exp. (3) and Exp. (5)) for real time experiments using on-line GC analysis. The purpose is to compare the performance (i.e. $H_2$ production and $CO_2$ adsorption) of catalysts with different supports in real time. The outlet compositions of $H_2$ and $CO_2$ under three catalysts were recorded by the instrument within 1 hour and are presented in Figure 5. The outlet compositions of other gases including CO, $CH_4$ and $N_2$ are neglected in Figure 5 in order to give a clearer interpretation.

According to Figure 5, when Ni-CaO is ued (Exp. (2)), the $H_2$ composition starts to increase with obvious trend at about 1001 s (17 mins) and reaches peak at about 1201 s (20 mins) at 36 mol%. Then the $H_2$ composition decreases rapidly to 7 mol% at 1601 s (27 mins). The $H_2$ composition continues decreasing until the end of experiment, which is only 2 mol% eventually. The $CO_2$ composition keeps at a low level from 0 mol% to 2 mol% throughout one-hour experiment time. As analysed before in s*ection 3.2*, Ni-CaO has very good $CO_2$ adsorption capability, which is consistent with the curve of $CO_2$ composition in Figure 5.

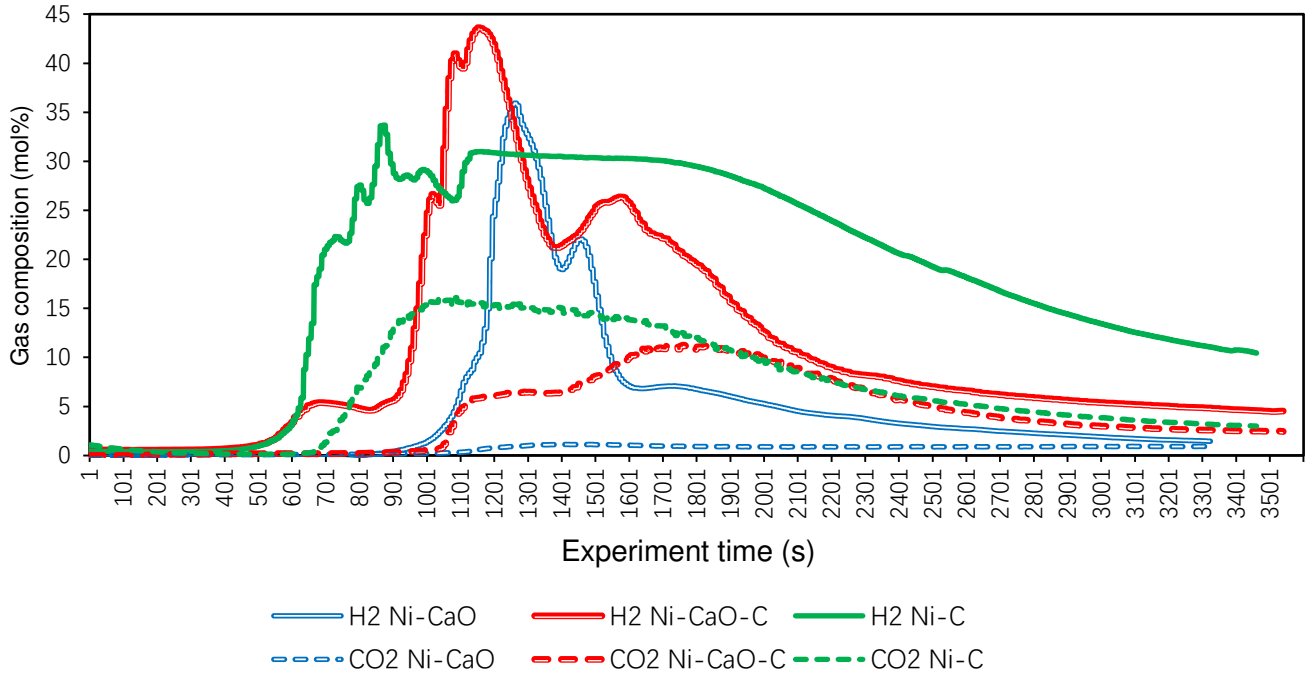


**Figure 5 Result of on-line GC analysis**

**(For all the catalysts: Ni load: 10 wt%, Biomass:Plastic=5:5, Pyrolysis T: 700 ºC, Reforming T: 600 ºC, Water: 5 mL/h)**

As for the curves of Ni-CaO-C (Exp. (5)), the $H_2$ composition begins to rise to 5 mol% since 601 s (10 mins), followed by a short time flat trend. Then $H_2$ composition increases sharply until the highest value 44 mol% at 1151 s (19 mins). At the end of the experiment, the $H_2$ composition stops at nearly 5 mol%. For $CO_2$, before 1001 s (17 mins), nearly no $CO_2$ is detected due to adsorption. A slight increase of $CO_2$ occurs due to promotion of relevant reactions generating $CO_2$ after 1001s (17 mins). Another obvious flat trend of $CO_2$ composition could be observed from 1101 s to 1401 s. This flat trend implies that a dynamic equilibrium is achieved between the $CO_2$ adsorption and $CO_2$ generation from reactions in reforming stage. Later, $CO_2$ generation gradually exceeds $CO_2$ adsorption by CaO. This may be because CaO is saturated. The $CO_2$ composition starts to increase slightly.

A great increase of $H_2$ composition occurs very early from 601 s (10 mins) when Ni-C (Exp. (3)) was used. The highest $H_2$ composition is 34 mol% and the $H_2$ composition keeps at a high level (over 30 mol%) for a long duration from 1101 s (19 mins) to 1901 s (32 mins). Even at the end of experiment, the $H_2$ composition is still nearly 10 mol%, which is the highest end composition among three catalysts. The $CO_2$ composition increases to a high level 15 mol% quickly at about 1001s (17 mins) and gradually decreases with a very slow pace until the experiment end. It could be observed that both $H_2$ and $CO_2$ compositions keep at high levels and last for long duration, demonstrating the good catalytic activity of Ni-C.

To compare the experiment results when using three different catalysts, the following findings are summarised:

(1) The peak $H_2$ composition comes the first when using the Ni-C catalyst, while the peak $H_2$ composition comes the last when using Ni-CaO catalyst. This phenomenon can be explained as the following: compared to activated carbon, the lack of catalytic activity of CaO results in low reaction rates, which delays the progress of $H_2$ generation reactions (e.g. reforming reactions).

(2) The case using Ni-CaO catalyst has the lowest $CO_2$ composition and the case using Ni-C catalyst has the highest $CO_2$ composition throughout the experiment. The

399 experiment results are consistent with the average $CO_2$ composition obtained from
400 GC in *section 3.2* as shown in bottom panel of Figure 3.
401 (3) The highest $H_2$ composition is achieved when using Ni-CaO-C among three
402 catalysts. This peak may be due to the synergetic effect of activated carbon and CaO
403 as discussed in *section 3.3*.
404 (4) The catalyst Ni-C has the longest time to promote reactions and the largest area
405 under the curve of $H_2$ composition which represents the $H_2$ yields. On the contrary,
406 Ni-CaO has the shortest time to promote reactions and the smallest area under the
407 curve of $H_2$ composition.
408 (5) The catalyst Ni-CaO-C combines the characteristics of Ni-CaO and Ni-C at the
409 same time. A trade-off is achieved appropriately between promoting $H_2$
410 composition and yield as a result.

411 **4. Life time analysis of catalyst Ni-CaO-C and catalyst regeneration**

412 **4.1 Life time analysis**

413 The life time analysis was carried out in the same reactor (see Figure 6) to examine
414 the continuous operation time for catalyst with a high catalytic performance. This is a
415 method to assess the stability of catalyst. 1.0 g catalyst Ni-CaO-C (Ni 10 wt% and
416 CaO:C=5:5) with 0.5 g feedstock (Biomass:Plastic = 5:5) were selected for analysis.
417 The operating procedures are the same as those introduced in *section 2.3*. For each cycle,
418 after feedstock was totally consumed, the reactor was cooled down. $N_2$ was kept
419 injecting into reactor to prevent oxidation of catalyst in bottom stage. Until the reactor
420 reached room temperature, new feedstock (0.5 g) was replaced at top stage again in
421 order to start a new cycle. The $H_2$ yield was measured and shown in Figure 6.

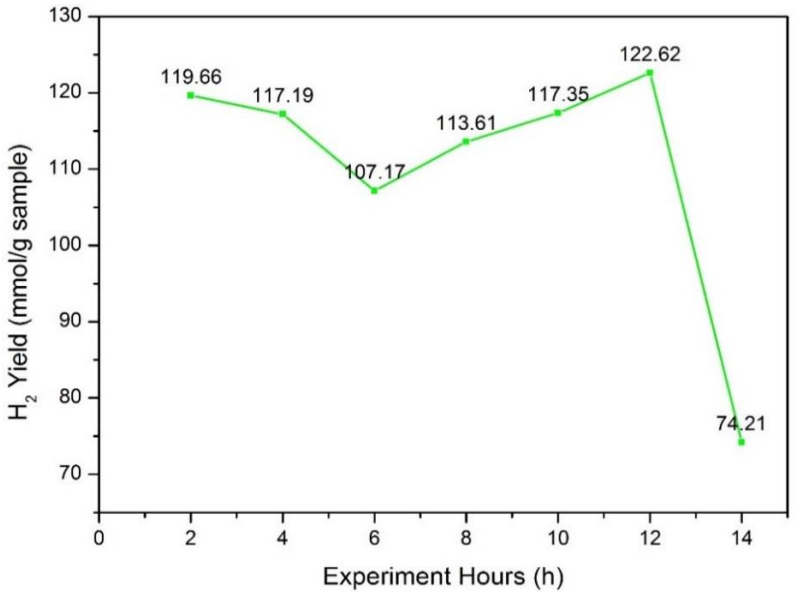


**Figure 6 Results of life time analysis**
**(with Ni load: 10 wt%, CaO:C=5:5, Biomass:Plastic =5:5, Pyrolysis T: 700 ºC, Reforming T: 600 ºC, Water: 5 mL/h)**

In Figure 6, it can be observed that the $H_2$ yield is nearly stable at the average value of 115 mmol/g before 12 h experiment. The stability of Ni-CaO-C is acceptable, which can be continuously operated for 12 h with relatively high $H_2$ yield. After 12 h, the $H_2$ yield starts to decrease sharply. With experiment time increase, coke is generated and deposits on the catalyst surface to decrease the catalytic activity. In addition to coke, generated tar is another important factor causing catalyst deactivation (Cortazar et al., 2018; Lopez et al., 2018). A high stability could help to decrease the frequency of catalyst regeneration, which is important for industrial application to decrease the operation cost.

### 4.2 Regeneration of used catalyst

Generally, used catalysts need to be regenerated due to low activity. In the papers of Clough et al. (2018) and Baidya and Cattolica (2015), Ni-CaO and Ni-CaO-Fe catalysts were used respectively. They performed regeneration by calcining the used catalysts under high temperature with air. The regenerated catalysts all have relatively high activity. From the results presented in Figures 8 (a) and (b), it is suggested to burn used Ni-CaO-C catalyst at least over 800 ºC. This is to ensure completed combustion of both deposited coke and activated carbon, and also entire conversion of $CaCO_3$ into CaO. The regenerated catalyst can be used in two forms: (1) It can be directly used as Ni-

CaO catalyst for pyrolysis/gasification. (2) It can be used as the precursor for preparation of new Ni-CaO-C catalyst by introducing activated carbon through impregnation method. In addition, the activated carbon can also be substituted by other carbon material such as biochar, which is much cheaper. This is our future direction to improve the catalyst furthermore.

Energy balance calculation is also performed for the process of catalyst regeneration. In order to simplify the calculation, some assumptions were made: (1) Assuming 1 g of used catalyst (i.e. Ni-CaO-C, Ni 10 wt%; CaO:C=5:5) is used for regeneration after Exp. (5). The used catalyst is calcined under 800 ºC with air; (2) Assuming all the NiO in used catalyst is totally reduced into Ni during pyrolysis/gasification; (3) Assuming only $CaCO_3$ exists in used catalyst (no CaO exists); (4) Assuming the coke deposit on the used catalyst surface is carbon, which is calculated with activated carbon together. The coke deposit ratio is assumed to be the same as the one (i.e. 0.53 wt%) in *section 5.1*; (5) Assuming all the chemical reactions are completed at their specific reaction temperatures. The calculation results are shown in Figure 7. The whole catalyst regeneration is a heat release process (releasing around 12,497 J when regenerating 1 g of used catalyst) due to combustion of activated carbon and deposited coke. This implies that a heat recovery process is necessary for catalyst regeneration process in practical application. The heat recovered from catalyst regeneration could be reused for other steps such as heating the feedstocks in reactors to maintain pyrolysis/gasification process. It should be noted that this energy balance calculation is simplified under the assumptions made above.

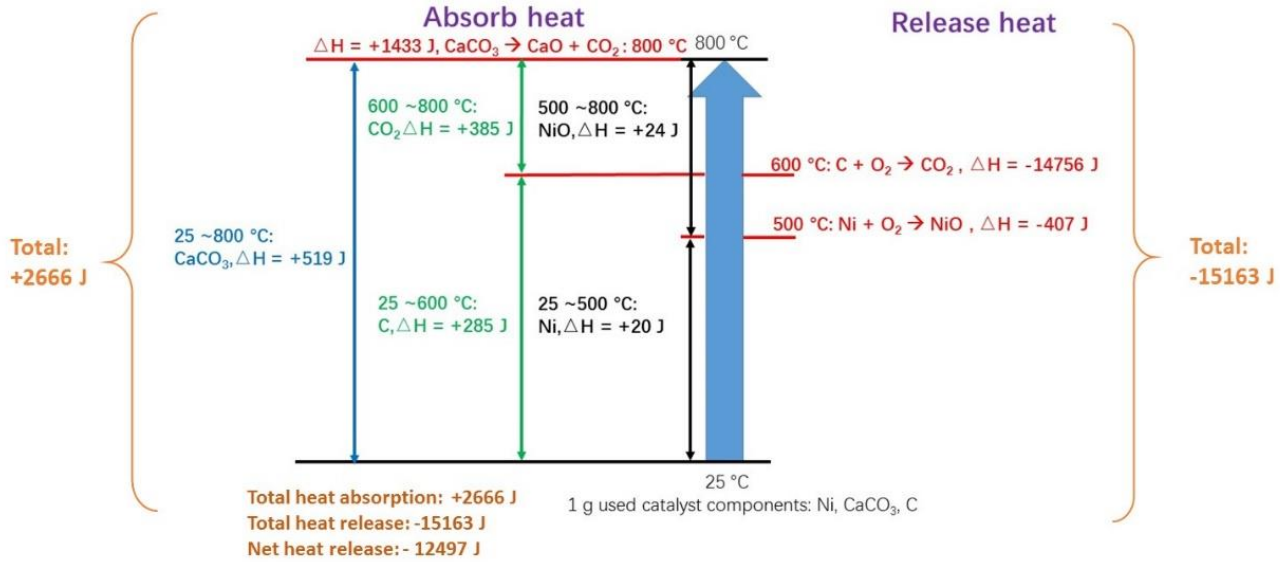


**Figure 7 Results of energy balance calculation for catalyst regeneration**

## 5. Characterisation of catalysts

In this study, TGA was carried out on used catalysts to detect the coke formation. XRD analysis was used to detect the specific chemicals on the surface of both fresh and used catalysts. SEM and EDX analysis were used to investigate the microstructure and element distribution on the surface of used catalysts. TPR analysis was used to detect the reducibility of fresh catalysts. Results from these characterisation analyses can help to explain the previous experimental results in *sections 3*.

### 5.1 TGA of used catalyst

In *section 3.2*, the influence of support ratio in catalyst was investigated. The used catalysts from Exp. (2), (3), (5), (8) and (9) were selected for TGA.

From Figure 8(a), with activated carbon content increase in the catalyst, the eventual weight ratio decreases. This is because that TG analysis was carried out under air. Activated carbon and coke were combusted. The more carbon the catalyst contains, the less weight the catalyst preserves after combustion.

For the catalyst Ni-CaO, two obvious weight loss stages can be observed at about 420 ºC and 620 ºC respectively. This is consistent with the observations from Wu et al. (2013). In Wu et al. (2013), two oxidation stages starting at 410 ºC and 600 ºC were

observed. According to their explanation, two kinds of carbon were generated and deposited on the catalyst as coke. Amorphous carbon was firstly combusted from 410 ºC and then filamentous carbon was combusted at higher temperature from 600 ºC. For the catalyst with dual-support, similar trends with two weight loss stages were observed. For catalyst Ni-C, only one weight loss stage was observed. This might be due to the activated carbon and the coke generated burn at the same temperature range.

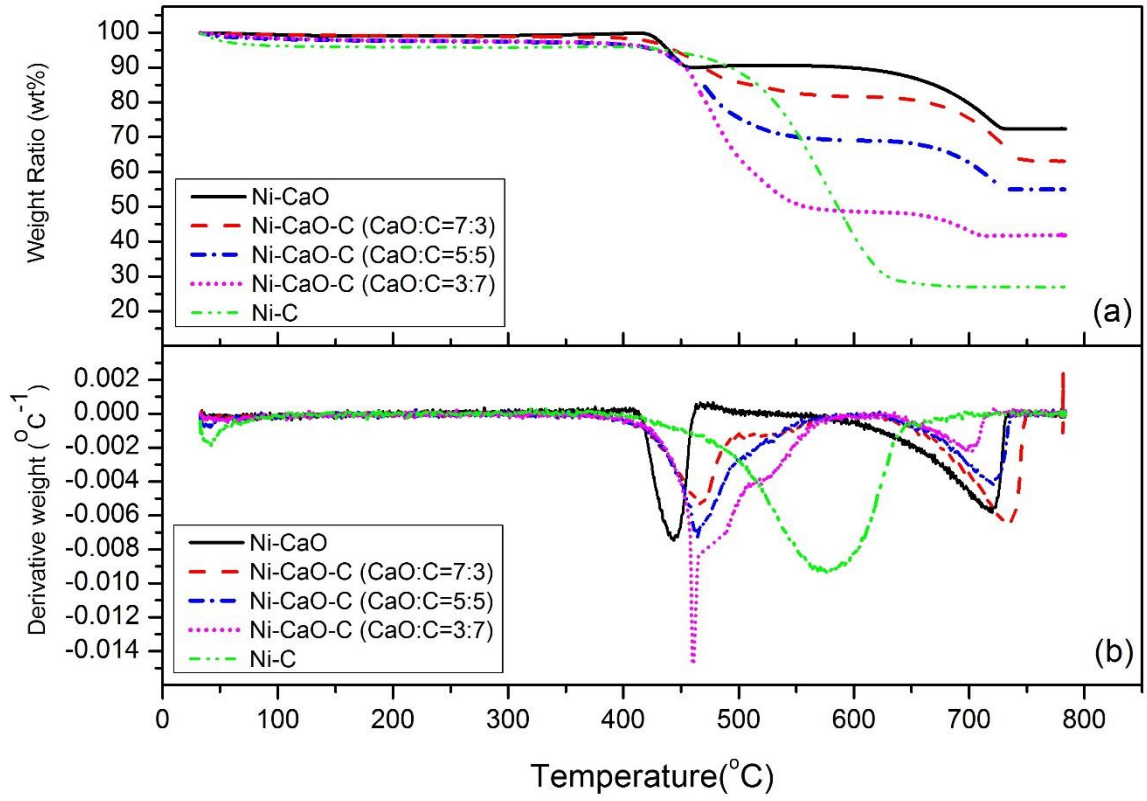


**Figure 8 Results of TG analysis of used catalysts (a) Weight ratio (b) Derivative weight (Foe all the cases: Ni load: 10 wt%, Biomass:Plastic=5:5, Pyrolysis T: 700 ºC, Reforming T: 600 ºC, Water: 5 mL/h)**

From Figure 8(b), derivative weight is the derivation of weight ratio in Figure 8(a), which can be used to reflect the weight loss peak of coke on catalyst surface. Except for Ni-C, the other catalysts all have two weight loss peaks. The weight loss peak of amorphous carbon of Ni-CaO occurs at the lowest temperature. The introduction of activated carbon increases the combustion temperature of amorphous carbon. Therefore, the combustion temperature for the coke deposited on the catalyst Ni-CaO-C surface will be higher. This may be one disadvantage of the Ni-CaO-C catalyst.

Coke deposit ratio is calculated based on the initial weight of used catalyst for TGA

to reflect extent of coke deposit. Due to existence of activated carbon in double-support catalysts, it is hard to distinguish the specific weight loss of activated carbon and coke from Figure 8. Therefore, weight loss ratios of fresh Ni-CaO-C (CaO:C including 3:7, 5:5 and 7:3) catalysts were also measured through TGA when there is no coke depositing on the catalyst. Then, specific coke deposit ratios were calculated using the weight loss ratio of used catalyst to minus the weight loss ratio of fresh catalyst. The coke deposit ratios for Ni-CaO-C (CaO:C=3:7), Ni-CaO-C (CaO:C=5:5) and Ni-CaO-C (CaO:C=7:3) are 5.50 wt%, 0.53 wt% and 0.32 wt% respectively.

### 5.2 XRD analysis of fresh and used catalysts

XRD analysis was applied for three different kinds of catalysts including Ni-CaO, Ni-CaO-C (Ni 10 wt% and CaO:C=5:5) and Ni-C. Both fresh and used catalysts were tested. The used catalysts were from three experiments (i.e. Exp. (2), Exp. (3) and Exp. (5)).

#### 5.2.1 Ni-CaO

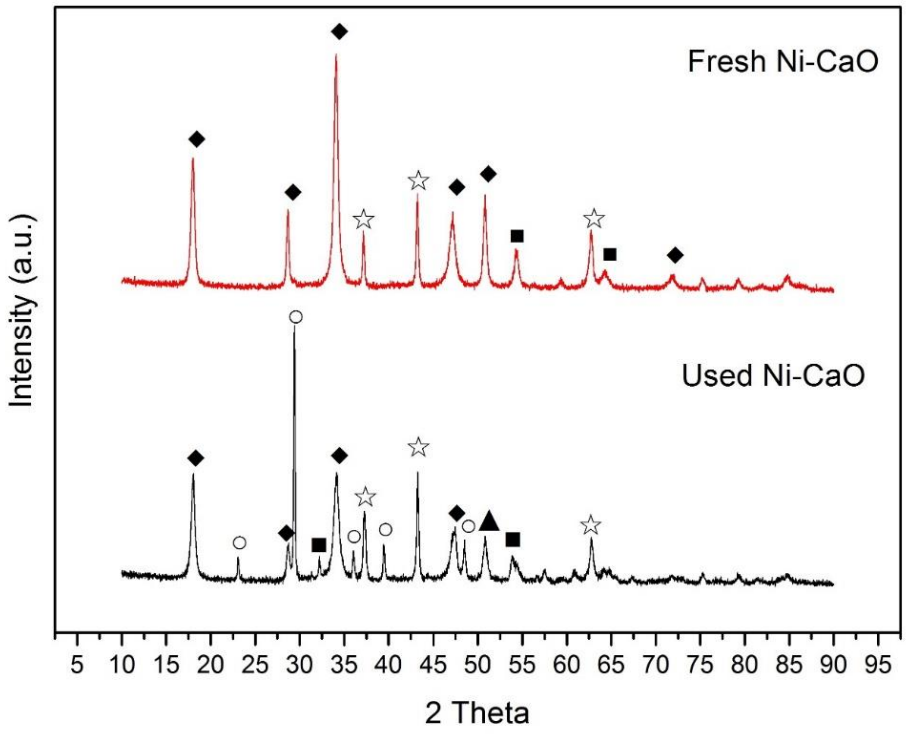


**Figure 9. Results of XRD analysis (◆Ca(OH)$_2$, ☆NiO, ■CaO, ○CaCO$_3$, ▲Ni)**

**(For both cases: Ni load: 10 wt%, CaO:C = 10:0, Biomass:Plastic=5:5, Pyrolysis T: 700 ºC, Reforming T: 600 ºC, Water: 5 mL/h)**

From top panel of Figure 9, Ca(OH)$_2$, CaO and NiO exist in the fresh catalyst. CaO

and NiO serve as catalyst support and active core respectively. $Ca(OH)_2$ is formed because CaO is sensitive to adsorb moisture in atmosphere. During experiments, the pre-heating process of reforming stage enables the conversion of $Ca(OH)_2$ into CaO. $Ca(OH)_2$ is decomposed to generate CaO and $H_2O$ between 520 – 580 ºC (see *Reaction 7*).

$$\mathbf{Ca(OH)_2 \rightarrow CaO + H_2O} \qquad \textbf{Reaction 7}$$

From bottom panel of Figure 9, in comparison with top panel, Ni and $CaCO_3$ only appear on the used Ni-CaO catalyst. Other components $Ca(OH)_2$, CaO and NiO are also detected on used Ni-CaO catalyst, same as in fresh catalyst. $Ca(OH)_2$ might be formed after experiments during equipment cooling or following catalyst characterisation. $CaCO_3$ is formed from CaO after adsorbing $CO_2$ (*Reaction 6*). It should be noted that the $CaCO_3$ in the used catalyst indicates the $CO_2$ adsorption capability of CaO in catalyst. This is consistent with the low $CO_2$ composition when using Ni-CaO catalyst in Figures 3 (bottom panel) and 5 in *section 3*. In addition, NiO exists in both fresh and used Ni-CaO catalysts to serve as the active core and NiO is only reduced to form Ni during pyrolysis/gasification process when contacting $H_2$.

### 5.2.2 Ni-CaO-C

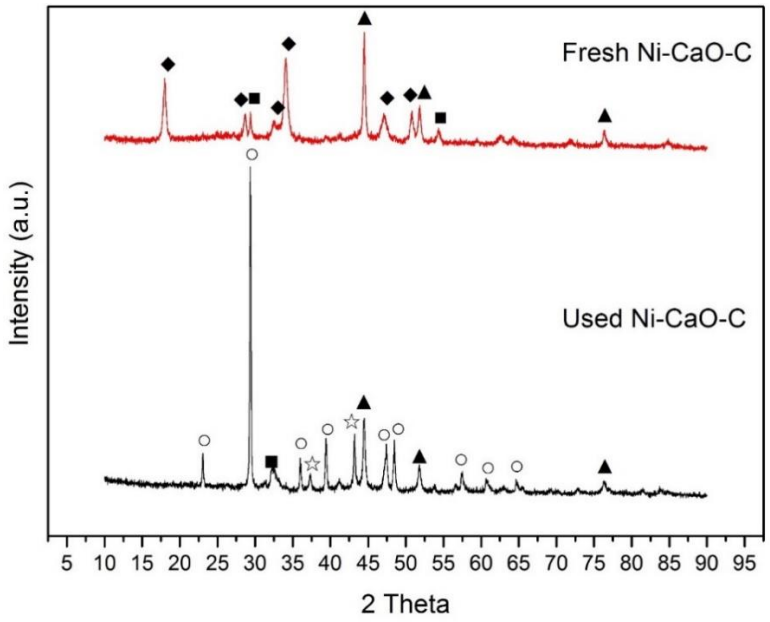


**Figure 10. Results of XRD analysis (◆Ca(OH)₂, ☆NiO, ■CaO, ○$CaCO_3$, ▲Ni)**

**(For two cases: Ni load: 10 wt%, CaO:C = 5:5, Biomass:Plastic=5:5, Pyrolysis T: 700 ºC, Reforming T: 600 ºC, Water: 5 mL/h)**

From top panel of Figure 10, $Ca(OH)_2$, CaO, NiO and Ni exist in the fresh Ni-CaO-C catalyst. Because of the reduction ability of activated carbon, some NiO could be reduced to form Ni during catalyst calcination process under high temperature. $Ca(OH)_2$, CaO, NiO, Ni and $CaCO_3$ exist in the used Ni-CaO-C catalyst. Similarly, the existence of $CaCO_3$ is only observed in used catalyst, which demonstrates the $CO_2$ adsorption capability of CaO in the catalyst Ni-CaO-C.

In comparison between the XRD results of fresh Ni-CaO (Figure 9) and Ni-CaO-C (Figure 10) catalysts, Ni only exists in fresh Ni-CaO-C catalyst. No activated carbon is comprised in Ni-CaO, thus no reduction ability could be offered to reduce NiO during catalyst calcination. Ni has better catalytic activity than NiO. Consequently, besides better pore structure and active in reforming stage, another advantage of activated carbon is reduction of NiO to Ni to promote $H_2$ yield. This is consistent with the results of $H_2$ yield in previous experimental studies (i.e. Exp. (2) and (5)), the $H_2$ yield using Ni-CaO is much lower than that of Ni-CaO-C in Figure 3 in *section 3.2*.

### 5.2.3 Ni-C

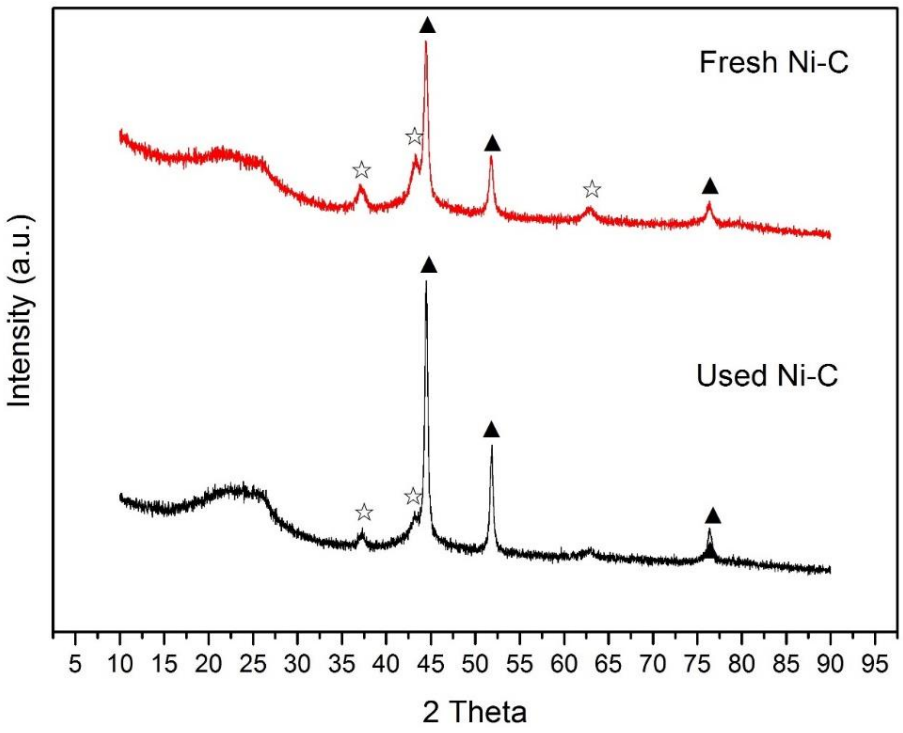


**Figure 11 Results of XRD analysis (☆NiO, ▲Ni)**
**(For two cases: Ni load: 10 wt%, CaO:C = 0:10, Biomass:Plastic=5:5, Pyrolysis T: 700 ºC, Reforming T: 600 ºC, Water: 5 mL/h)**

From Figure 11, only Ni and NiO are detected in both used and fresh Ni-C catalysts. NiO is also reduced to generate Ni during catalyst calcination process. Compared to fresh Ni-CaO-C catalyst (top panel in Figure 10), the highest Ni intensity at 45 degrees on fresh Ni-C catalyst is higher, which means a better crystallinity degree and formation trend of Ni particle (Hu et al., 2009). This may be due to the higher content of activated content in Ni-C catalyst, enabling a better reduction of NiO during catalyst calcination. As a result, catalyst Ni-C possesses better catalytic activity. This is consistent with the results in Figure 3 in *section 3.2* that using Ni-C (Exp. (2)) has the highest total gas yield and $H_2$ yield.

### 5.3 SEM analysis of used catalyst and BET analysis of fresh catalyst

Fresh catalysts Ni-CaO, Ni-CaO-C (CaO:C=5:5) and Ni-C were selected for BET analysis to detect the specific surface area. The specific results of BET analysis are shown in Table 5.

**Table 5 Results of BET analysis**

| Catalysts | Specific surface area ($m^2/g$) | Total pore volume ($cm^3/g$) |
|---|---|---|
| Ni-CaO | 7.632 | 0.172 |
| Ni-CaO-C | 542.565 | 0.306 |
| Ni-C | 1365.448 | 0.619 |

From Table 5, it can be observed that Ni-CaO has the lowest specific surface area and total pore volume among three catalysts. Ni-C has the highest specific surface area and total pore volume. This is resulted from the better porous structure of activated carbon compared to CaO.

The used catalysts for SEM analysis come from experimental studies in *section 3.2*. Catalysts from Exp. (2), (3), (5), (8) and (9) were selected. All the figures (Figure 12) from SEM analysis were obtained with the same magnification (50.00 k x).

From Figure 12 (a), when only CaO is used as support in catalyst, layer structure is dominant, which is guessed to be CaO or coke deposited on the catalyst surface. When CaO is 70 wt% of the catalyst support, the pore structure is still not obvious in Figure 12 (b). With CaO content decrease and activated carbon content increase in catalyst,

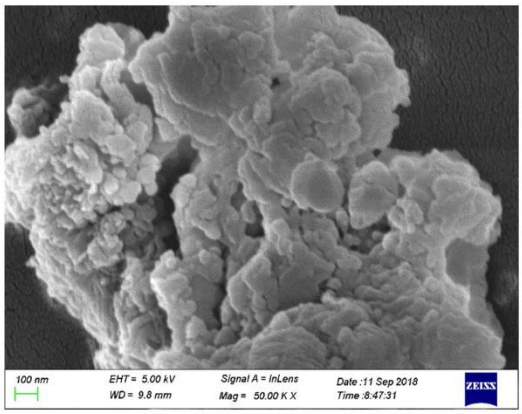


(a) Ni-CaO (Ni 10 wt%)

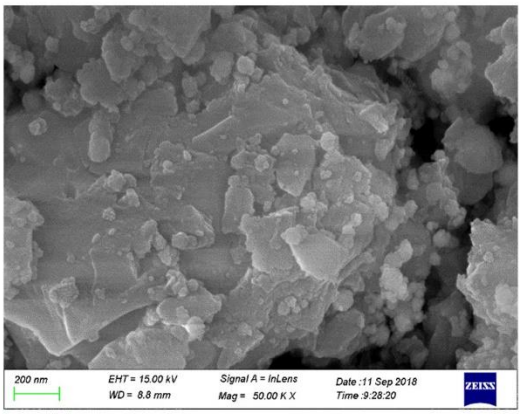


(b) Ni-CaO-C (Ni 10 wt%, CaO:C=7:3)

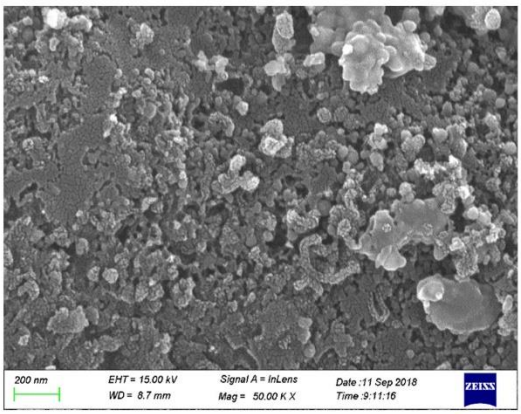


(c) Ni-CaO-C (Ni 10 wt%, CaO:C=5:5)

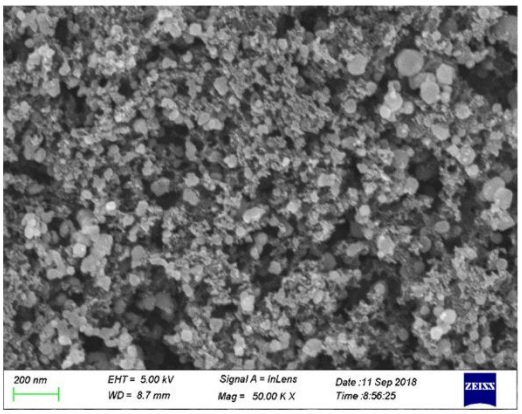


(d) Ni-CaO-C (Ni 10 wt%, CaO:C=3:7)

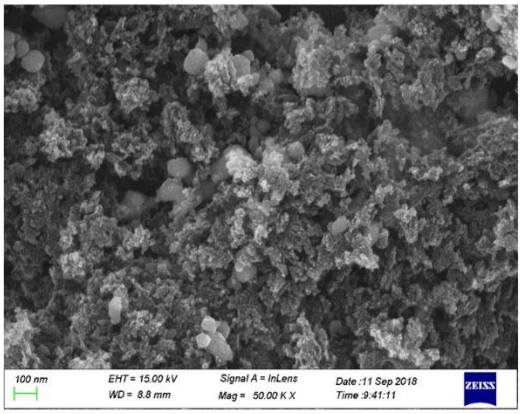


(e) Ni-C (Ni 10 wt%)

**Figure 12 Results of SEM analysis**
**(Fall all the cases: Ni load: 10 wt%, Biomass:Plastic=5:5, Pyrolysis T: 700 ºC, Reforming T: 600 ºC, Water: 5 mL/h)**

pore structure is observed more obviously in Ni-CaO-C (CaO:C=5:5) in Figure 12 (c). Eventually, when activated carbon is dominant in Figure 12 (d) and 12 (e), abundant pore structures are provided.

In summary, with activated carbon content increase in catalyst, better pore structure is provided, which increases the specific area of catalyst. Consequently, the cracking reactions as well as reforming reactions can be promoted. The results in Table 5 and Figure 12 are consistent with the results in Figure 3 in *section3.2*.

**5.4 EDX analysis of used catalyst**

Only the catalyst of Exp. (5) was used for EDX analysis. The EDX results of used catalyst Ni-CaO-C (CaO:C=5:5) are shown in Figure 13. In Figure 13, relatively uniform distribution of four kinds of elements can be observed on the catalyst surface. On one hand, this proves the perfect distribution of active core Ni on the two supports. On the other hand, the two kinds of supports (i.e. CaO and activated carbon) seem to be well mixed. C is relatively more accumulated at the right side of catalyst. Correspondingly, less Ni is observed at the same area. Coke is predicted to be deposited in this area, which results in a higher content of C.

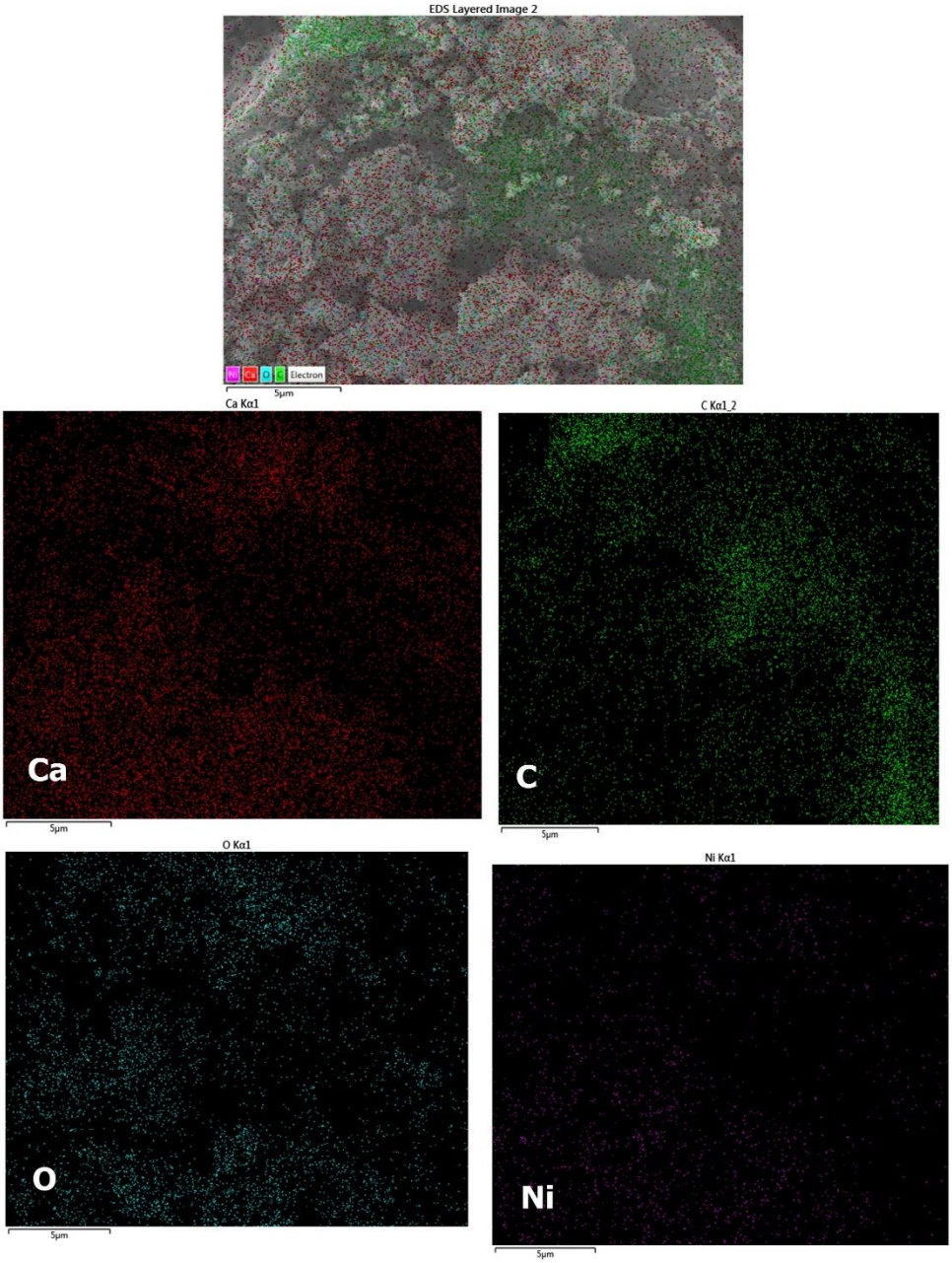


**Figure 13 Results of EDX analysis**
**(Ni load: 10 wt%, CaO:C = 5:5, Biomass:Plastic = 5:5, Pyrolysis T: 700 ºC, Reforming T: 600 ºC, Water: 5 mL/h)**

## 5.5 TPR analysis of fresh catalyst

The fresh catalysts used in TPR analysis come from experimental studies in *section 3.2.* Catalysts from Exp. (2), (3), (5), (8) and (9) were selected.

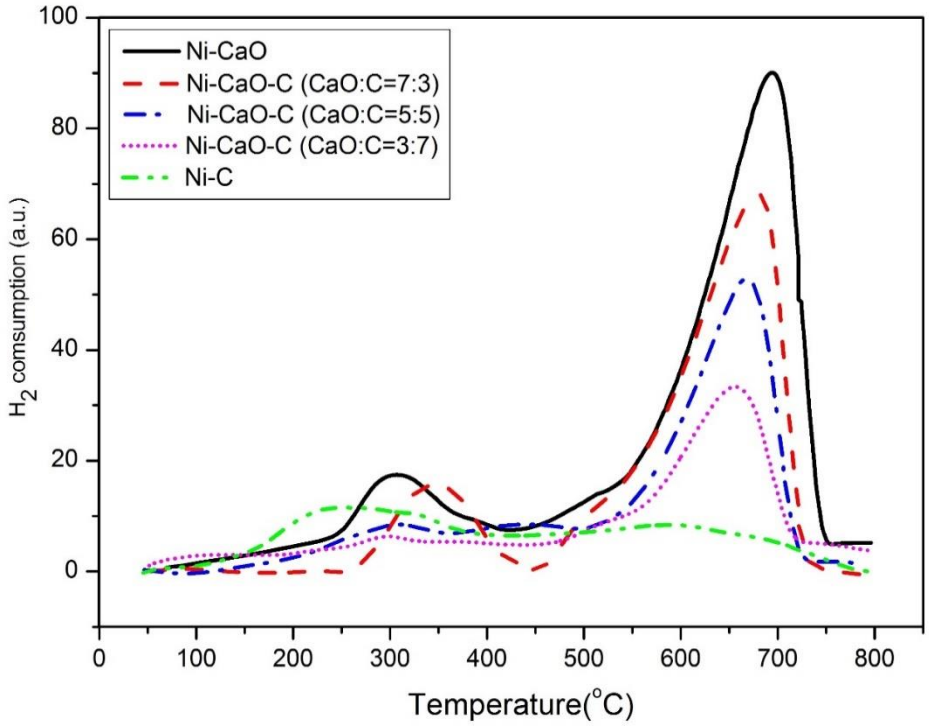


**Figure 14 Results of TPR analysis**

**(For all the cases: Ni load: 10 wt%, Biomass:Plastic (weight ratio) =5:5, Pyrolysis T: 700 ºC, Reforming T: 600 ºC, Water: 5 mL/h)**

From Figure 14, for Ni-CaO and Ni-CaO-C (CaO:C=7:3), they both have two obvious $H_2$ consumption peaks due to the different crystalline phase structures of NiO on the catalyst surface. The higher peaks occur in 600 – 700 ºC, which represents the main reduction process of majority of NiO on catalysts. For Ni-CaO-C (CaO:C=5:5) and Ni-CaO-C (CaO:C=3:7), only one obvious peak can be observed in 600 – 700 ºC. For Ni-C, no obvious peak is observed in 600 – 700 ºC. To analyse the $H_2$ consumption of different catalysts in 600 – 700 ºC, Ni-CaO has the highest $H_2$ consumption. With activated carbon content increase in the catalyst, the $H_2$ consumption keeps decreasing. The less $H_2$ consumption represents that more NiO in fresh catalysts has already been converted into Ni. It is because that activated carbon itself has reduction ability. During the catalyst calcination process, activated carbon can reduce NiO to form Ni. This is consistent with the results of XRD analysis in *section 5.2*. In *section 5.2*, Ni is only observed in the fresh catalysts Ni-CaO-C and Ni-C and no Ni is observed in fresh Ni-CaO.

## 6. Experimental studies on optimal operating conditions when using the catalyst Ni-CaO-C (Ni 10 wt%, CaO:C=5:5)

In this section, 8 different experiments (as listed in Table 6) were carried out to find optimal operating conditions. Optimal operating conditions (i.e. feedstock ratios, pyrolysis temperature, reforming temperature and water injection flowrate) are defined as a combination of the following:

(1) A higher $H_2$ yield is selected when the $H_2$ composition in the products is higher than 80 mol%.

(2) The lower operation costs the better, this implies lower operating temperature and lower water injection flowrate

**Table 6 List of experiments for optimal operating conditions**

| Exp.Number | (11) | (12) | (13) | (14) | (15) | (16) | (17) | (18) |
|---|---|---|---|---|---|---|---|---|
| Feedstock ratio Biomass:Plastic (weight ratio) | 3:7 | 7:3 | 5:5 | 5:5 | 5:5 | 5:5 | 5:5 | 5:5 |
| T of pyrolysis stage(ºC) | 700 | 700 | 600 | 800 | 700 | 700 | 700 | 700 |
| T of reforming stage(ºC) | 600 | 600 | 600 | 600 | 500 | 700 | 600 | 600 |
| Water injection flowrate (mL/h) | 5 | 5 | 5 | 5 | 5 | 5 | 1 | 10 |

### 6.1 Influence of feedstock ratio on $H_2$ composition and yield

The results presented in Figure 15 were from Exp. (5), Exp. (11) and Exp. (12). From Figure 15, when 30 wt% plastics is used in feedstock, the $H_2$ composition is 70.34 mol%. With more plastics is introduced in feedstock (i.e. 50 wt% and 70 wt%), the $H_2$ compositions also increase to 86.74 mol% and 91.42 mol%. It can be concluded that higher plastic content in feedstock results in higher $H_2$ composition. According to Alvarez et al. (2014), plastics is rich in H content, which results in a higher H/C molar ratio than that of biomass. The abundant H element in plastics provides more H donors for $H_2$ formation. Thus more hydrogen is generated and the concentration of $H_2$ elevates.

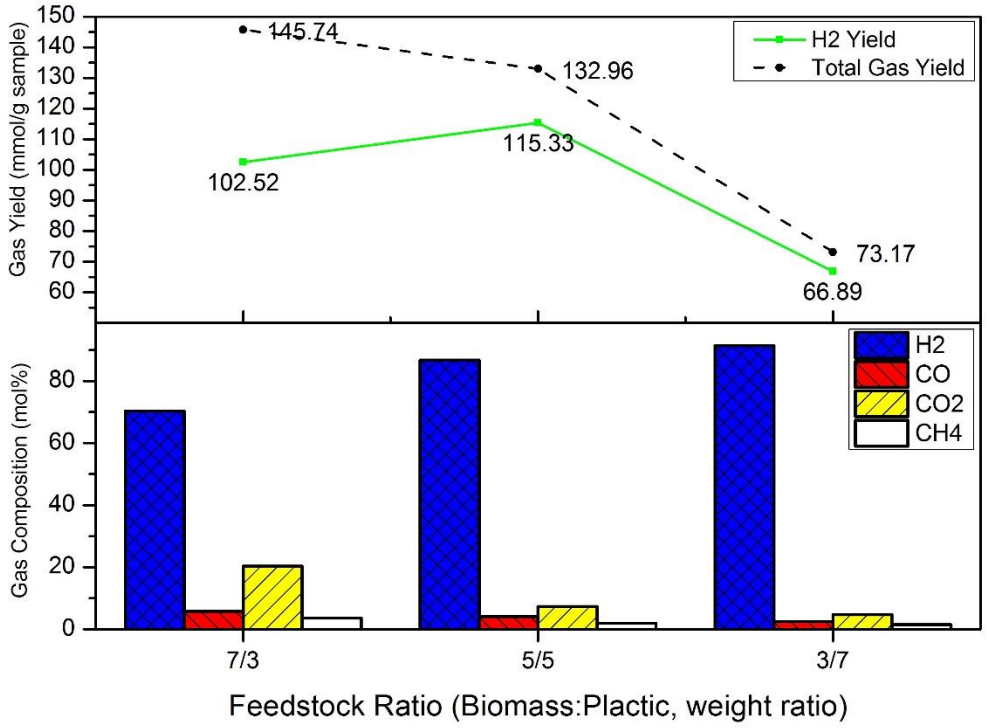


**Figure 15 Gas compositions and yields changing with feedstock ratio (For all 3 cases: Ni load: 10 wt%, CaO:C = 5:5, Pyrolysis T: 700 ºC, Reforming T: 600 ºC, Water: 5 mL/h)**

As for $H_2$ yield, when the plastic content increases from 30 wt% to 50 wt%, the $H_2$ yield increases from 102.52 mmol/g to 115.33 mmol/g. However, further increasing plastic content (70 wt%) results in reduction of $H_2$ yield to 66.89 mmol/g. A similar trend about decreasing $H_2$ yield with higher plastic content over 70 wt% could be found in the study of Ahmed et al. (2011). A probable explanation might be due to the synergetic effect of biomass and plastics. The H donors from plastic not only form $H_2$, but also react with radicals from biomass. The reactions between H donors and radicals promote cracking of complicated components (e.g. aromatics) from biomass (Burra and Gupta, 2018), releasing more simple hydrocarbons (e.g. lighter hydrocarbons such as $CH_4$ and C2~C3) and CO (Abdelouahed et al., 2012). As another source of H element, $H_2O$ will further react with the generated lighter hydrocarbons and CO through reforming reactions to produce more $H_2$. If the plastic content is too high in the feedstock mixture, insufficient radials are offered to generate less hydrocarbons and CO due to lack of biomass, resulting in restrictions of cracking and reforming reactions. As a result, the $H_2$ yield decreases at a higher plastic content in feedstock.

## 6.2 Influence of pyrolysis/reforming temperature

Previous studies indicated that temperature is an important factor to influence the product yields (Pinto et al., 2003; Brachi et al., 2014). In those two studies, pyrolysis/gasification take place at the fixed bed reactor or fluidised reactor. For two-stage fixed bed reactor used in this study, it is even more convenient to implement separate temperature control of pyrolysis and reforming stages, which enables to investigate the specific influences of temperature at different stages clearly.

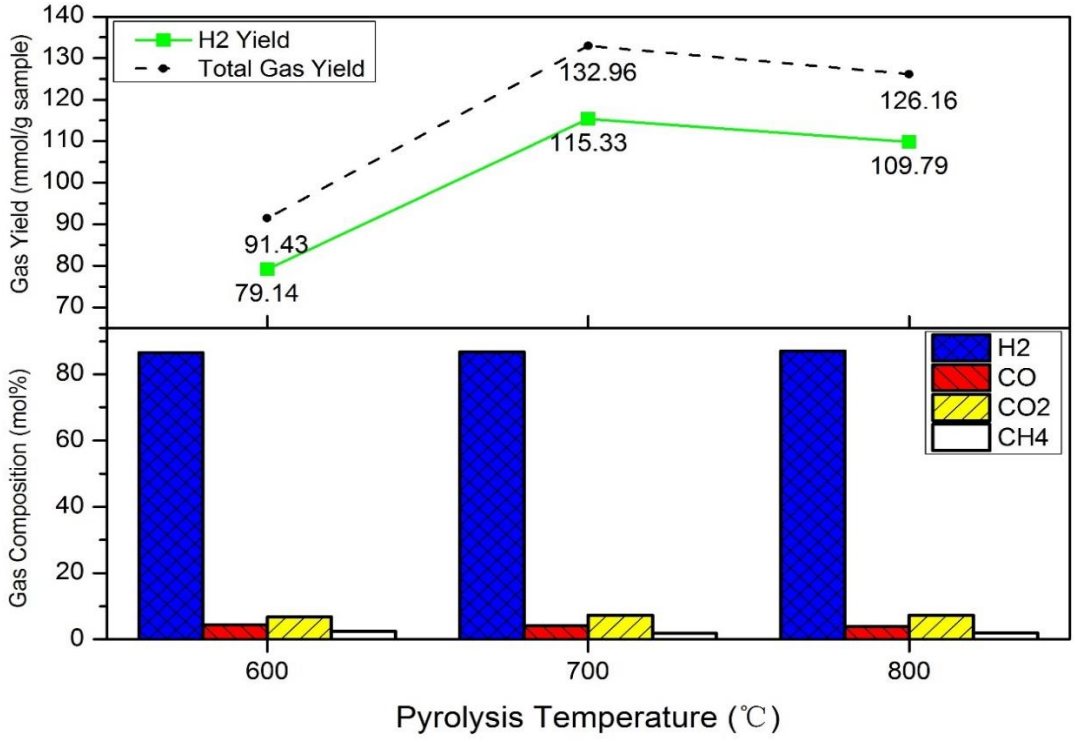


**Figure 16 Gas compositions and yields changing with pyrolysis temperature (For all 3 cases: Ni load: 10 wt%, CaO:C = 5:5, Biomass:Plastic=5:5, Reforming T: 600 ºC, Water: 5 mL/h)**

The results presented in Figure 16 were from Exp. (5), Exp. (13) and Exp. (14). From Figure 16, the compositions of four main gas products do not change significantly when pyrolysis temperature increases from 600 ºC to 800 ºC. Pyrolysis is a kind of decomposition process and no complicated reactions (like reforming reactions) take place in this stage to influence eventual gas compositions. Consequently, the gas compositions under different temperatures do not change much.

The $H_2$ yield firstly goes up from 79.14 mmol/g at 600 ºC to 115.33 mmol/g at 700 ºC, and then decreases to 109.79 mmol/g when temperature rises to 800 ºC. Pyrolysis is endothermic, which is beneficial under a higher temperature. A better decomposition

extent of feedstock is advantageous to provide sufficient reactants for the bottom reforming stage. That is the reason why the $H_2$ yield is higher in higher temperatures (600 ºC and 700 ºC) compared to 500 ºC.

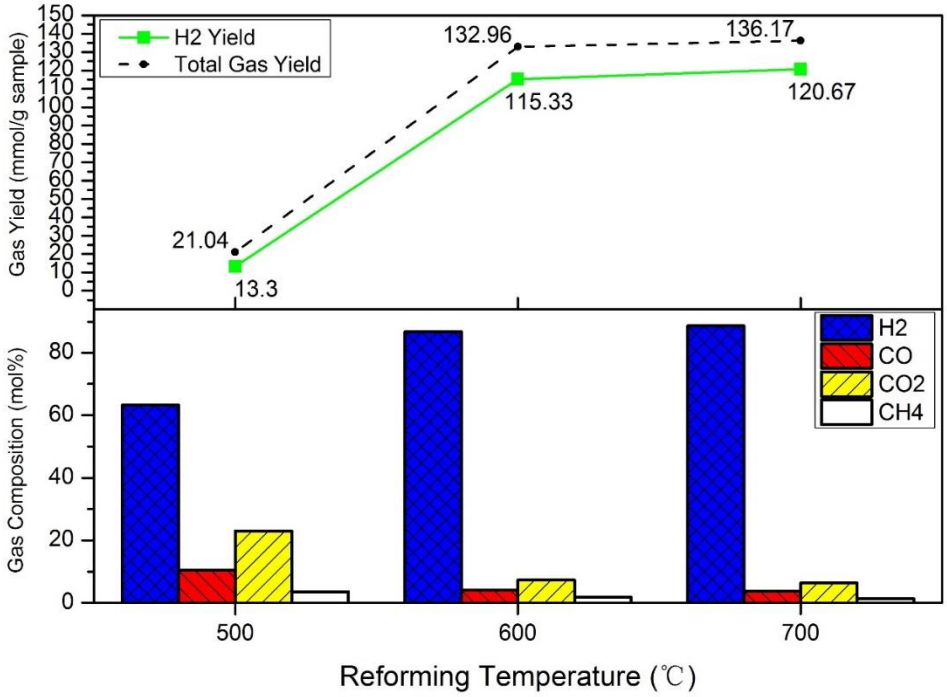


**Figure 17 Gas compositions and yields changing with reforming temperature (For all 3 cases: Ni load: 10 wt%, CaO:C = 5:5, Biomass:Plastic=5:5, Pyrolysis T: 700 ºC, Water: 5 mL/h)**

The results presented in Figure 17 were from Exp. (5), Exp. (15) and Exp. (16). From Figure 17, when the reforming temperature is 500 ºC, the $H_2$ composition and yield are 63.19 mol% and 13.30 mmol/g. With reforming temperature increase to 600 ºC, both $H_2$ composition and yield experience dramatic enhancement, which are 86.74 mol% and 115.33 mmol/g. Further increase of temperature to 700 ºC results in 88.62 mol% of $H_2$ composition and 120.67 mmol/g of $H_2$ yield.

Both $H_2$ composition and yield benefit from higher reforming temperature, which is consistent with previous studies (Wu and Williams, 2010b; Pinto et al., 2002). 500 ºC is not an appropriate temperature for normal function of Ni-CaO-C catalyst. The low temperature of reforming stage restricts the activity of Ni-CaO-C catalyst since both WG reaction (*Reaction 1*) and SMR reaction (*Reaction 5*) are endothermic reactions. Higher temperatures (i.e. 600 ºC and 700 ºC) tend to move the reaction equilibrium towards generating more $H_2$. Thus increasing $H_2$ composition and yield are achieved

under higher temperature. In addition, SMR reaction consumes $CH_4$ to produce $H_2$. This is consistent with the $CH_4$ composition changes in Figure 17, which keeps decreasing along with increase of temperature and $H_2$ composition. However, compared to the increase between low temperature interval (i.e. from 500 ºC to 600 ºC), the promotion effects under higher temperature (i.e. from 600 ºC to 700 ºC) is very limited. This might be attributed to the restriction of WGS reaction (*Reaction 4*). WGS reaction is an exothermic reaction and a higher temperature moves the reaction equilibrium towards generating less $H_2$. That is the reason why less promotion effect is observed at much higher temperature.

### 6.3 Influence of water injection flowrate

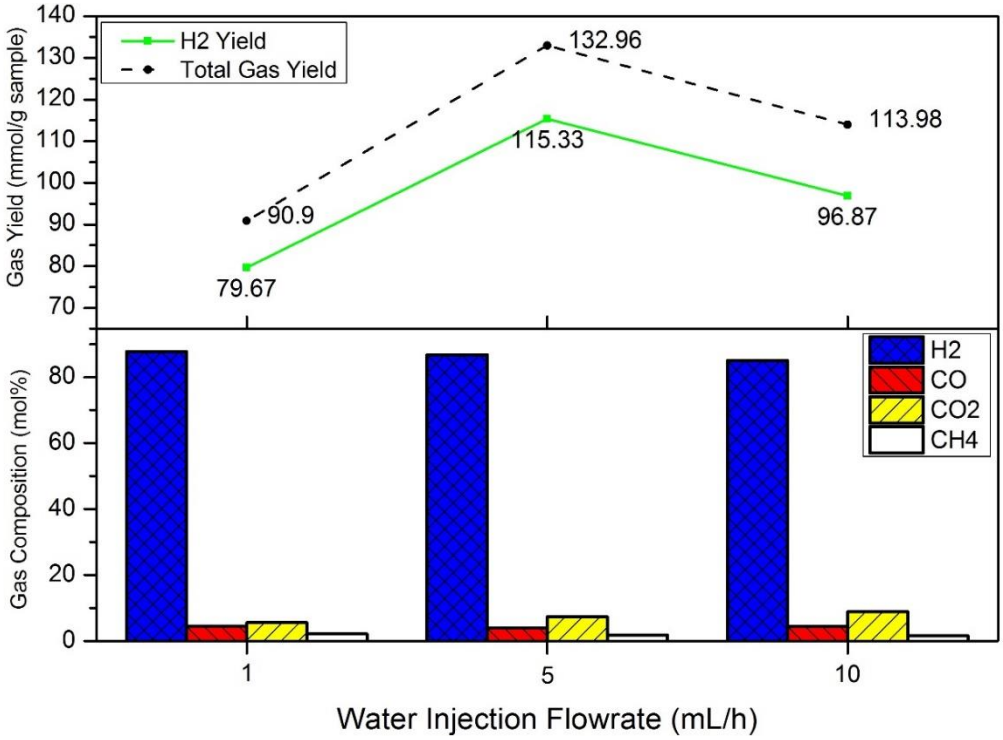


**Figure 18 Gas compositions and yields changing with water injection flowrate (For all 3 cases: Ni load: 10 wt%, CaO:C = 5:5, Biomass:Plastic=5:5, Pyrolysis T: 700 ºC, Reforming T: 600 ºC)**

The results presented in Figure 18 were from Exp. (5), Exp. (17) and Exp. (18). From Figure 18, when the water injection flowrate is 1 mL/h, $H_2$ composition is 87.65 mol%. Further increase of flowrate to 5 and 10 mL/h has slight influences on the $H_2$ composition, which are 86.74 and 84.99 mol%. In general, increase of water injection has negligible effect to change gas compositions. This is consistent with the results of

731 Pinto et al. (2002).

732 The $H_2$ yield is 79.67 mmol/g when 1 mL/h water is injected. Higher $H_2$ yield is
733 realised at 115.33 mmol/g with 5 mL/h water injection. Further increase of water to 10
734 mL/h decreases the $H_2$ yield to 96.87 mmol/g. Compared to $H_2$ composition, the $H_2$
735 yield has more obvious changes. An increasing trend of $H_2$ yield is firstly observed in
736 the range of 1 mL/h to 5 mL/h water injection. It is because that introduction of more
737 water is advantageous to WGS reaction (*Reaction 4*), whose equilibrium moves toward
738 generating more $H_2$. However, a further increase of water injection hinders the $H_2$ yield.
739 Li et al. (2012) once used steam gasification technology to treat MSW (including
740 mixture of biomass and plastics) and Acharya et al. (2010) investigated steam
741 gasification of biomass for $H_2$ production in the presence of CaO. In their studies,
742 higher water injection leads to $H_2$ yield decreasing. A probable explanation could be
743 that the excessive water in the system may absorb considerable heat inside the reactor.
744 This hinders normal decomposition of feedstock in the pyrolysis stage and restricts
745 smooth progress of some reactions in the reforming stage (Li et al., 2012). Consequently,
746 a lower total gas yield including $H_2$ is obtained under an excessively higher water
747 flowrate.

748 **6.4 Summary of optimal operating conditions**

749 Through these experiments using the newly synthesised catalyst Ni-CaO-C (Ni 10
750 wt% CaO:C=5:5, the optimal operating conditions are found to be:

751 (1) Feedstock ratio (i.e. biomass: plastic 5:5), pyrolysis temperature 700 ºC and water
752 injection flowrate 5 mL/h are selected due to high $H_2$ composition (over 80 mol%) and
753 the highest $H_2$ yield in the product stream.

754 (2) Reforming temperature 600 ºC: Although the $H_2$ composition and yield of 700 ºC
755 are higher than that of 600 ºC, the differences are very small. Considering the practical
756 operation cost under high temperature, 600 ºC is selected as the optimal operating
757 condition.

758 Under the optimal operating conditions, the $H_2$ composition and yield are 86.74 mol%
759 and 115.33 mmol/g respectively as shown in Figure 3.

## 7. Conclusions

In this paper, a new catalyst Ni-CaO-C was developed for pyrolysis/gasification of of plastics (i.e. LDPE) and pine sawdust for $H_2$ production. Ni load and support ratio (i.e. CaO:C) were changed during pyrolysis/gasification experiments using a 2-stage fixed bed reactors in order to explore catalytic activity and $CO_2$ adsorption capability of the new catalyst. Experimental results indicate that the new catalyst combines high catalytic activity and $CO_2$ adsorption capability, thus it promotes $H_2$ production with both high $H_2$ composition and yield. As explored in this study, this is caused by synergy between Ni (active core), CaO ($CO_2$ adsorption) and activated carbon (active in reforming reactions, massive pore structure and good reduction ability). Life time analysis indicates the stability of the newly developed catalyst. Characterisation of fresh and used catalysts demonstrated that the new catalyst will result in low coke formation. The new catalyst will generate better pore structure and higher surface area. These characterisation results can help to explain why the new catalyst has better catalytic performance. Operating conditions (such as feedstock ratio, pyrolysis/gasification temperatures and water injection flowrate) were also tested experimentally. The optimal operating conditions using the new catalyst for pyrolysis/gasification of biomass and plastics are 10 wt% Ni, CaO:C =5:5, biomass : plastics =5:5, pyrolysis temperature 700 ºC, reforming temperature 600 ºC and water injection flowrate 5 mL/h. Under the optimal operating conditions, the specific $H_2$ composition and $H_2$ production are 86.74 mol% and 115.33 mmol/g respectively and $CO_2$ composition in the gas products is only 7.31 mol%. This study points to new direction for $H_2$ production from the pyrolysis/gasification of waste plastics and biomass.

## Acknowledgement

The authors would like acknowledge the financial support of the EU H2020 Research and Innovation Staff Exchange (RISE) programme with project title "*Development of flexible pyrolysis-catalysis processing of waste plastics for selective production of high*

*value products through research and innovation*" (Ref: 643322-FLEXI-PYROCAT), National Natural Science Foundation of China (51476023, 51306029), China Postdoctoral Science Foundation (2016M600790, 2016M602828) and Key Research and Development Plan of Shaanxi Province (2017GY-167).

**References**

Abdelouahed, L., Authier, O., Mauviel, G., Corriou, J.P., Verdier, G., Dufour, A. (2012), Detailed modeling of biomass gasification in dual fludized bed reactors under Aspen Plus, *Energy & Fuels*, 26, pp.3840 – 3855.

Acharya, B., Dutta, A., Basu, P. (2010), An investigation into steam gasification of biomass for hydrogen enriched gas production in presence of CaO, *International Journal of Hydrogen Energy*, 35, pp.1582-1589.

Ahmed, I.I., Nipattummakul, N., Gupta, A. K. (2011), Characteristics of syngas from co-gasification of polythelene and woodchips, *Applied Energy*, 88, pp.165-174.

Alvarez, J., Kumagai, S., Wu, C.F., Yoshioka, T., Bilbao, J., Olazar, M., Williams, P.T. (2014), Hydrogen production from biomass and plastic mixtures by pyrolysis-gasification, *International Journal of Hydrogen Energy*, 39, pp. 10883-10891.

Al-Rahbi, A.S., Williams, P.T. (2017), Hydrogen-rich syngas production and tar removal from biomass gasification using sacrificial tyre pyrolysis char, *Applied Energy*, 190, pp. 501 – 509.

Baidya, T., Cattolica, R.J. (2015), Fe and CaO promoted Ni catalyst on gasifier bed material for tar removal from producer gas, *Applied catalysis A: General*, 503, pp. 43-50.

Basu, P (2013), Biomass Gasification and Torrefaction, 2nd Ed. Elsevier.

Block, C., Ephraim, A., Hortala, E.W., Minh, D.P., Nzihou, A., Vandecasteele, C. (2018), Co-pyrogasification of plastic and biomass, a review, *Waste and Biomass Valorization*, 10.1007/s12649-018-0219-8.

Brachi, P., Chirone, R., Miccio, F., Picarelli, A., Ruoppolo, G. (2014), Fluidized bed co-

817 gasification of biomass and polymeric wastes for a flexible end-use of the syngas: focus
818 on bio-methanol, *Fuel*, 128, pp.88-98.
819 Brems, A., Dewil, R., Baeyens, J., Zhang, R. (2013) Gasification of plastic waste as
820 waste-to-energy or waste-to-syngas recovery route, *Natural Science*, 5(6), pp. 695-704.
821 Burra, K.G., Gupta, A.K. (2018), Synergistic effects in steam gasification of combined
822 biomass and plastic waste mixtures, *Applied Energy*, 211, pp. 230 – 236.
823 Cho, M.H., Choi, Y.K., Kim, J.S. (2015), Air gasification of PVC (polyvinyl chloride)-
824 containing plastic waste in a two-stage gasifier using Ca-based additives and Niloaded
825 activated carbon for the production of clean and hydrogen-rich producer gas, *Energy*,
826 87, pp.586-593.
827 Clough, P.T., Boot-Handford, M.E., Zheng, L.Y., Zhang, Z.L., Fennell, P.S. (2018),
828 Hydrogen production by sorption enhanced steam reforming (SESR) of biomass in a
829 fluidised-bed reactor using combined multifunctional particles, *Materials*, 11(5),
830 pp.859 - 882.
831 Cortazar, M., Alvarez, J., Lopez, G., Amutio, M., Santamaria, L., Bilbao, J., Olazar, M.
832 (2018), Role of temperature on gasification performance and tar composition in a
833 fountain enhanced conical spouted bed reactor, *Energy Conversion and Management*,
834 171, pp.1589-1597.
835 Czajczyńska, D., Anguilano, L., Ghazal, H., Krzyzynska, R., Reynolds, A.J., Spencer,
836 N., Jouhara, H. (2017) Potential of pyrolysis processes in the waste management sector,
837 *Thermal sicence and engineering progress*, 3, pp. 171 – 197.
838 Déparrois, N., Singh, P., Burra, K.G., Gupta, A.K. (2019), Syngas production from co-
839 pyrolysis and co-gasification of polystyrene and paper with $CO_2$, *Applied Energy*, 246,
840 pp. 1 – 10.
841 Gao, N.B., Han, Y., Quan, C. (2018), Study on steam reforming of coal tar over Ni-
842 Co/ceramic foam catalyst for hydrogen production: effect of Ni/Co ratio,
843 *International Journal of Hydrogen Energy*, 43, pp. 22170 – 22186.
844 Himan, C., Burdgt, M.A.D. (2008), Gasification, 2nd ed., Gulf Professional Publishing.
845 Hu, G.X., Huang, H. (2009), Hydrogen rich fuel gas production by gasification of wet

846 biomass using a $CO_2$ sorbent, *Biomass and Energy*, 33, pp.899-906.
847 Jacoobson, M.Z. (2008), Review of solutions to global warming, air pollution, and
848 energy security, *Energy & Environmental Science*, 2, pp.148-173.
849 Kumagai, S., Alvarez, J., Blanco, P.H., Wu, C. F., Yoshioka, T., Olazar, M., Williams,
850 P.T. (2015), Novel Ni-Mg-Al-Ca catalyst for the enhanced hydrogen production for the
851 pyrolysis-gasification of a biomass/plastic mixture, *Journal of Analytical and Applied*
852 *Pyrolysis*, 113, pp.15-21.
853 Kumar, A., Jones, D.D., Hanna, M.A. (2009), Thermochemical Biomass Gasification:
854 A review of the Current Status of the Technology, *Energies*, 2, pp.556-581.
855 Kwon, B.W., Oh, H.J., Kim, G.S., Yoon, S.P., Han, J. (2018), The novel perovskite-type
856 Ni-doped $Sr_{0.92}Y_{0.08}TiO_3$ catalyst as a reforming biogas ($CH_4 + CO_2$) for $H_2$ production,
857 *Applied Energy*, 227, pp. 213 – 219.
858 Li, J.F., Liao, S.Y., Dan, W.Y., J, K.L., Zhou, X.R. (2012), Experimental study on
859 catalytic steam gasification of municipal solid waste for bioenergy production in a
860 combined fixed bed reactor, *Biomass and Bioenergy*, 46, pp.174-180.
861 Liu, B.S., Au, C.T. (2003), Sol-gel-generated $La_2NiO_4$ for $CH_4/CO_2$ reforming,
862 *Catalysis Letters*, 85, pp. 165-170.
863 Liu, G.C., Liao, Y.F., Wu, Y.T., Ma, X.Q. (2018), Synthesis gas production from
864 microalgae gasification in the presence of $Fe_2O_3$ oxygen carrier and CaO additive,
865 *Applied Energy*, 212, pp. 955 – 965.
866 Lopez, G., Artetxe, M., Amutio, M., Alvarez, J., Bilbao, J., Olazar, M. (2018), Recent
867 advances in the gasification of waste plastics. A critical overview, *Renewable*
868 *Sustainable Energy Reviews*, 82, pp. 576-596.
869 Pinto, F., Franco, C., Andre, R.N., Miranda, M., Gulyurtlu, I., Cabrita, I. (2002), Co-
870 gasification study of biomass mixed with plastic wastes, *Fuel*, 81, pp.291-297.
871 Pinto, F., Franco, C., Andre, R.N., Tavares, C., Dias, M., Gulyurtlu, I., Cabrita, I. (2003),
872 Effect of experimental conditions on co-gasification of coal, biomass and plastics
873 wastes with air/steam mixtures in a fluidized bed system, *Fuel*, 82, pp.1967-1976.
874 Ren, J., Cao, J.P., Zhao, X.Y., Wei, F., Liu, T.L., Fan, X., Zhao, Y.P., Wei, X.Y. (2017),

875 Preparation of high-dispersion Ni/C catalyst using modified lignite as carbon precursor
876 for catalytic reforming of biomass volatiles, *Fuel*, 202, pp.345-351.
877 Sansaniwal, S.K., Pal, K., Rosen, M.A., Tyagi, S.K. (2017), Recent advances in the
878 development of biomass gasification technology: A comprehensive review, *Renewable*
879 *and Sustainable Energy Reviews*, 72, pp. 363-384.
880 Sikarwar, V.S., Zhao, M., Fennell, P.S., Shah, N., Anthony, E.J. (2017) Process in
881 biofuel production from gasification, *Progress in Energy and Combustion Science*, 61,
882 pp. 189-248.
883 Verma, R., Vinoda, K.S., Papireddy, M., Gowda, A.N.S. (2016), Toxic pollutants from
884 plastic waste – A Review, *Procedia Environmental Sciences*, 35, pp. 701-708.
885 Wu, C.F., Williams, P.T. (2009), Hydrogen production by steam gasification of
886 polypropylene with various nickel catalysts, *Applied Catalysis B: Environmental*, 87,
887 pp. 152-161.
888 Wu, C.F., Williams, P.T. (2010a), A novel Ni-Mg-Al-CaO catalyst with the dual
889 functions of catalysis and $CO_2$ sorption for $H_2$ production from the pyrolysis-
890 gasification of polypropylene, *Fuel*, 89, pp.1435-1441.
891 Wu, C.F., Williams, P.T. (2010b), Pyrolysis-gasification of post-consumer municipal
892 solid plastic waste for hydrogen production, *International Journal of Hydrogen Energy*,
893 35, pp.949-957.
894 Wu, C.F., Wang, Z.C., Dupont, V., Huang, J., Williams, P.T. (2013), Nickel-catalysed
895 pyrolysis/gasification of biomass components, *Journal of Analytical and Applied*
896 *Pyrolysis*, 99, pp.143-148.
897 Yang, R.X., Chuang, K.H., Wey, M.Y. (2018), Effects of temperature and equivalence
898 ratio on carbon nanotubes and hydrogen production from waste plastic gasification in
899 fluidized bed, *Energy Fuels*, 32, pp. 5462-5470.
900 Yao, Z.Y., You, S.M., Ge, T.S., Wang, C.H. (2018), Biomass gasification for syngas and
901 biochar co-production: Energy application and economic evaluation, *Applied Energy*,
902 209, pp. 43-55.
903 Zhang, W.D., Liu, B.S., Tian, Y.L. (2007), $CO_2$ reforming methane over Ni/$Sm_2O_3$-CaO

904 catalyst prepared by a sol-gel technique, *Catalysis Communications*, 8, pp. 661-667.
905 Zhao, X.L., Lv, Y.A., Liao, W.P., Jin, M.S., Suo, Z.H. (2015), Hydrogen production
906 from steam reforming of ethylene glycol over supported nickel catalysts, *Journal of*
907 *Fuel Chemistry and Technology*, 43(5), pp.581-588.
908 Zhou, H., Nebg, A.H., Long, Y.Q., Li, Q.H., Zhang, Y.G. (2014), Classification and
909 comparison of municipal solid waste based on thermochemical characteristics, *Journal*
910 *of the Air & Waste Management Association*, 64(5), pp.597-616.
911 Zhang, X.S., Lei, H.W., Chen, S.L., Wu, J. (2016), Catalytic co-pyrolysis of
912 lignocellulosic biomass with polymers: a critical review, *Green chemistry*, 18, pp. 4145
913 – 4169.